Journal Pre-proofs

Degradation of three typical hydroxamic acids collectors via UVA-B activated H_2O_2 and persulfate: Kinetics, transformation pathway, DFT calculation and toxicity evaluation

Wancheng Pang, Jun Yao, Tatjana Šolević Knudsen, Ying Cao, Bang Liu, Hao Li, Miaomiao Li, Junjie Zhu

PII: S1385-8947(22)04120-1
DOI: https://doi.org/10.1016/j.cej.2022.138639
Reference: CEJ 138639

To appear in: *Chemical Engineering Journal*

Received Date: 11 May 2022
Revised Date: 30 July 2022
Accepted Date: 12 August 2022

Please cite this article as: W. Pang, J. Yao, T. Šolević Knudsen, Y. Cao, B. Liu, H. Li, M. Li, J. Zhu, Degradation of three typical hydroxamic acids collectors via UVA-B activated H_2O_2 and persulfate: Kinetics, transformation pathway, DFT calculation and toxicity evaluation, *Chemical Engineering Journal* (2022), doi: https://doi.org/10.1016/j.cej.2022.138639

Degradation of three typical hydroxamic acids collectors via UVA-B activated H_2O_2 and persulfate: Kinetics, transformation pathway, DFT calculation and toxicity evaluation

Wancheng Pang[a], Jun Yao[a,*], Tatjana Šolević Knudsen[b], Ying Cao[a], Bang Liu[a], Hao Li[a], Miaomiao Li[a], Junjie Zhu[a]

[a] School of Water Resources and Environment, Research Center of Environmental Science and Engineering, China University of Geosciences (Beijing), 29 Xueyuan Road, Haidian District, Beijing 100083, China

[b] University of Belgrade, Institute of Chemistry, Technology and Metallurgy, Department of Chemistry, Njegoševa 12, 11000 Belgrade, Serbia

*Corresponding author.

E-mail addresses: yaojun@cugb.edu.cn (Jun Yao)

Abstract

This work systematically studied the kinetics and mechanism of degradation of salicylhydroxamic acid (SHA), benzhydroxamic acid (BHA) and N-hydroxyphthalimide (NOP) by UVA-B/H_2O_2 and UVA-B/peroxodisulfate (PDS). UVA-B irradiation could induce a direct photolysis of SHA and dominated SHA destruction in both systems. BHA and NOP were effectively degraded via $HO^{\bullet}$- and $SO_4^{\bullet-}$-mediated oxidation. UVA-B/PDS displayed a better degradation performance for HAAs investigated than UVA-B/H_2O_2. An acidic pH was more suitable for three HAAs removal in the UVA-B/H_2O_2 system. However, basic pH was more efficient for HAAs degradation in the UVA-B/PDS system. The degradation of BHA and NOP was predominantly driven by $SO_4^{\bullet-}$ at all pH levels used (5.0 - 9.0). The second-order rate constants for SHA, BHA and NOP reactions with $HO^{\bullet}$ and $SO_4^{\bullet-}$ were calculated to be (4.16 - 5.22) × 10^9 $M^{-1}\cdot s^{-1}$ and (1.19 - 7.22) × 10^9 $M^{-1}\cdot s^{-1}$, respectively. Presence of various water constituents had different influence on HAA removal, with a enhancement in the presence of HCO_3^-, Fe^{2+} and Cu^{2+}. When real waters were used as a background, dissolved organic carbon and Cl^- were the main factors that consumed radicals and affected the degradation performance of HAAs. Analysis of the transformation products and density functional theory revealed that all of the investigated HAAs first generated amidated products but the formation mechanisms might have been different. HAAs degradation pathways mainly included hydrolysis, hydroxylation, decarboxylation and ring opening processes. Toxicity evaluation showed that the UV/AOP degradation of HAAs generated some transformation products with higher acute toxicity than the parent compounds.

Key words: Hydroxamic acid; UVA-B irradiation; Degradation kinetics; Hydroxyl and sulfate radical; Transformation pathway;

1. Introduction

The development of highly industrialized world economy has led to an enormous burden on mine resources and the environment [1-2]. Excessive exploitation of minerals has led to the depletion of ore resources. Lean ore that is difficult to utilize is becoming the main source of some minerals [3]. Concerns of the decline in high grade mineral resources and ever-growing mineral consumption have resulted in the consumption of organic flotation agents for extraction of target metals that annually exceeds one million tons [4-5]. Over the past decades, several typical hydroxamic acids (RCONHOH) anionic collectors: salicylhydroxamic acid (SHA), benzhydroxamic acid (BHA) and N-hydroxyphthalimide (NOP) have been extensively used in flotation of oxidized copper minerals, scheelite, some rare earths and low grade niobium tailings [6-9], especially in the Gannan area of China [10]. The dosage of HAAs collector used usually 90 - 250 μM depending on the mineral deposit and flotation process, and approximately 35 - 100 μM residual HAAs end up in the industrial wastewater [11-14]. They can increase chemical oxygen demand content of wastewater [10, 15]. Moreover, the accumulation of nitrogen elements from HAAs in water can induce eutrophication and deteriorate water quality, thus posing adverse influences on the aquatic ecosystems [10, 15]. Hydroxamic acids have physiological toxicity due to the presence of a benzene ring in their structure. Among these three HAA flotation agents, NOP manifests toxicity, persistence, mutagenicity and carcinogenicity that are similar to other nitrogen-heterocyclic compounds [16]. Many studies have also reported that numerous synthetic hydroxamic acids have been shown to be highly mutagenic and carcinogenic [17]. Furthermore, residual flotation reagents might chelate metal ions from the tailings ponds, leading to an increased bioavailability and toxicity of metal, and causing secondary pollution [3, 18]. In this

context, investigation of processes and mechanisms for efficient removal of these hydroxamate collectors from the effluents, is of great significance for prevention of potential ecological and health risks.

Numerous researches have been conducted so far, which were aimed at the treatment of flotation reagents from mineral processing wastewaters using coagulation-sedimentation, biological treatment and advanced oxidation processes (AOPs). Although coagulation-precipitation and biological treatments are, to some extent, more cost-effective than AOP (Table S1), these methods have limitations, such as sludge generation which requires additional treatment, high input of chemicals, long treatment cycle and strict requirements that must be fulfilled to maintain microbial cultures active and viable [19-21]. Because of that, and due to their simplicity and high efficiency, AOPs have been regarded as an emerging and promising alternative [22-23]. Traditional AOPs typically involve the generation of non-selective hydroxyl radicals ($HO^{\bullet}$), which degrade recalcitrant organic pollutants in wastewaters via electron transfer, hydrogen abstraction or electrophilic addition reactions [24]. Sulfate radical-based AOPs have also attracted a lot of attention, because sulfate radical ($SO_4^{\bullet-}$) has a higher redox potentials (2.5 - 3.1 V) than $HO^{\bullet}$ (1.9 - 2.7 V) especially at higher pH values [25]. $SO_4^{\bullet-}$ can react with contaminants via electron transfer or H-abstraction, decarboxylation and hydroxylation reaction [26]. It has been reported that emerging pharmaceuticals, food dyes and herbicide can be effectively removed in $SO_4^{\bullet-}$-based AOPs [27-29]. Generally, the photo-activation in AOPs is driven by UVC radiation (254 nm) [30-31]. Nevertheless, in comparison with UVA-B radiations (280 - 400 nm), UVC lamps require higher energy and they are more expensive so their utilization is not suitable for long-term pollutant removal processes [31]. From an economical point of view, the use of UVA-B radiation can

reduce the operating cost and can even be replaced with the UV fraction of the solar light for a real-scale application, making it more sustainable. Studies employing UVA-B/AOP have been attracting increased interest because they have proved that these processes are efficient technology for the removal of various contaminants, such as plasticizer, hormones and flotation reagents [21, 30-31]. For example, Lu and coworkers reported a high efficiency of the UVA-B induced $S_2O_8^{2-}$ process for the oxidative degradation of a new flotation reagent α-Nitroso-β-naphthol [21].

Research regarding the removal of HAA in mineral processing wastewater is still quite limited. There are only a few reports focused on the preparation of photocatalytic material for degradation of HAA [10, 15, 18]. Nevertheless, these reports did not investigate the transformation mechanisms of HAA in great details. Some important details such as identification of the transformation products and evaluation of their toxicity, and the effects of some parameters such as pH, common water matrices, etc. are still unclear. At present, no systematic studies have investigated the degradation of HAA by UVA-B/AOP both, kinetically and mechanistically. In our present study, in order to elucidate degradation kinetics and the mechanism, three representative aromatic HAAs were selected as the target pollutants: BHA with the basic structure of HAAs, SHA with the phenolic hydroxyl structure and NOP with the nitrogen-heterocyclic structure (Table S2). These model compounds are expected to provide valuable reference for degradation of other HAAs collectors by UV/AOP.

Considering all aforementioned facts, the objectives of the present work were to: (1) explore the influence of typical parameters (including the oxidant dosage, pH and water matrices) on the reaction kinetics during the UVA-B/H_2O_2 and UVA-B/PDS degradation processes of SHA, BHA and NOP; (2) determine the roles of active

species ($HO^{\bullet}$ and $SO_4^{\bullet-}$) and the second rate constants in degradation reactions of the target contaminants; (3) assess the degradation performance of three HAAs in two types of real waters; (4) conduct product analysis coupled with density functional theory (DFT) in order to provide insights into the reaction mechanisms and pathways of HAAs, which is essential for the toxicity assessment.

2. Materials and methods

2.1 Chemicals and materials

The specific information about all chemicals used in this study can be found in Text S1 of the Supplementary Material.

2.2. Experimental setup for photochemical procedures

A BL-GH-V photoreactor (Bilon, Shanghai, China) was utilized for the UVA-B/AOP destruction experiments of SHA, BHA and NOP. UVA-B radiation was sourced from a UV mercury lamp equipped with a filter that provides light in the wavelength range from 280 to 400 nm. The reaction mixture temperature was maintained at 20 ± 1°C using a cooling system. The solution pH was maintained using a 2 mM phosphate buffer solution. Except when otherwise stated, the photochemical experiment was conducted in a solution containing H_2O_2 or PDS at 1.8 mM and HAA (i.e. SHA, BHA and NOP) at 60 μM, and at initial pH of 7.0 ± 0.1. At predefined time intervals, 1.0 mL of the solution was withdrawn from the reaction mixture, 50 μL of methanol was added to quench the residual radicals and the sample was immediately sent for further analysis. Dark controls were included in each batch of the samples, and no loss of HAAs was found in the dark. All experiments were conducted in duplicate or triplicate.

2.3. Analytical methods

The quantitative details of SHA, BHA, NOP, benzoic acid (BA) and nitrobenzene (NB) were listed in Text S2 and Table S3. The analytical method used for identification of the transformation products (TPs) is described in Text S2. The free radical species were identified by Electron spin resonance (EPR) spectra (A300 EPR Spectrometer, Bruker, Germany). The DFT calculation method using ORCA software (Version 4.2) and Multiwfn software is provided in Text S3 [32-34]. Total organic carbon (TOC) was measured via a TOC analyzer (Shimadzu TOC-L, Japan). The acute toxicity of untreated and UVA-B/AOP treated HAAs samples was assessed by the evaluation of luminescence inhibition of the marine bacterium *Vibrio fischeri* [35]. The luminescence intensity was determined photometrically using a Microtox® Model 500 Analyzer (Modern Water, Cambridge, UK). The ecological structure-activity relationship (ECOSAR) program was applied to evaluate the acute and chronic toxicities of HAAs and their transformation products (TPs) at three trophic levels of aquatic organisms [36].

3. Results and discussion

3.1. Comparison of HAAs degradation by UVA-B/ H_2O_2 and UVA-B/PDS oxidation

The HAAs removal in the UVA-B/AOP systems followed pseudo-first-order reaction kinetics. The obtained degradation rates and pseudo-first-order degradation rate constants (k_{obs}) of HAAs investigated at various H_2O_2 and PDS dosages are clearly depicted in Fig. 1. During UVA-B irradiation, SHA was rapidly photodegraded with a k_{obs} of 0.0980 min^{-1} (Fig. 1a). In contrast, no measurable direct photolysis of BHA and NOP was observed during UVA-B irradiation (Fig. 1b-c). It has been reported for direct photolysis that the emission spectra of the light source ought to overlap with the absorption spectra of the target contaminants [37]. Absorption spectra of SHA presents a major absorption band in the UVA-B region

(294 nm, Fig. S1), corresponding to $\pi \rightarrow \pi^*$ transition. However, strong absorption bands in this region were not found in BHA and NOP spectra. This observation reveals that the probability for direct photolysis of SHA is much higher than that for the other two HAAs. Moreover, hydroxyl (-OH) substituents present in SHA molecule are electron-donating groups capable of increasing electron density of the aromatic ring. This feature might make SHA more susceptible to excitation and more photosensitive [38]. During the UVA-B exposures, a remarkable degradation of HAAs was observed in the H_2O_2 and PDS reactions and the removal rates increased as the oxidant concentrations increased (Fig. 1). These results imply that H_2O_2 and PDS can be UVA-B photochemically activated to degrade HAAs through production of highly oxidative radical species (R S1-2, Table S4). Similar result was found by Huang et al., who indicated that UVA-B fraction of solar light could efficiently activate PDS and H_2O_2 resulting in the removal of Bisphenol-A [30].

With the H_2O_2 concentration increase from 0.6 to 2.4 mM, the k_{obs} of BHA increased from 0.0106 to 0.0231 min^{-1}; the k_{obs} of NOP increased from 0.0052 to 0.0121 min^{-1}. However, as the H_2O_2 concentration increased, SHA removal did not correspondingly enhance as expected and the k_{obs} (0.0959 - 0.1016 min^{-1}) remained almost the same as the rate constants of direct photolysis. It is generally accepted that higher $HO^{\bullet}$ levels are generated with increased initial H_2O_2 concentration in the UV/H_2O_2 system. Accordingly, the authors reasonably speculated that in the reaction of $HO^{\bullet}$ with SHA the reaction rate constant might be much lower than that of direct photolysis. From this point on, the discussion on SHA degradation will mainly address the effect of the direct photolysis and UVA-B/PDS treatment. Regarding the UVA-B/PDS system, with increase in PDS concentration from 0.6 to 2.4 mM, the k_{obs} of SHA, BHA and NOP degradation increased from 0.1068, 0.0178 and 0.0093 min^{-1}

to 0.1519, 0.0520 and 0.0355 min^{-1}, respectively. It is obvious that the removal efficiency of UVA-B/PDS process was always higher than that in UVA-B/H_2O_2 process at the same oxidant ratio. Such discrepancy might be ascribed to the following mechanisms: First, the O–O bond in $S_2O_8^{2-}$ is longer and has lower energy than the O–O bond in H_2O_2. As a result, under UVA-B irradiation PDS is activated more easily than H_2O_2 and the apparent quantum yield of PDS photolysis is higher than that of H_2O_2 photolysis [21]. Second, the self-recombination of $SO_4^{\bullet-}$ and the reaction of $SO_4^{\bullet-}$ with its precursor are much slower than that of $HO^{\bullet}$ (R S3-4, Table S4) [39]. Consequently, $SO_4^{\bullet-}$ in the UVA-B/PDS process is produced more efficiently than $HO^{\bullet}$ in the UVA-B/H_2O_2 process.

3.2 Effect of pH

To study the effect of pH on the process efficiency, a series of degradation experiments was conducted with 60 μM HAAs at pH values of 5.0, 7.0 and 9.0. The results are plotted in Fig. 2. It can be noticed that at the end of the treatments with UVA-B only (20 min), the photolytic removal of SHA at pH values of 5.0, 7.0 and 9.0 reached 76.93%, 86.09% and 93.13%, while the corresponding k_{obs} were 0.0722, 0.0980 and 0.1337 min^{-1}, respectively (Fig. 2a). Many reports have indicated that the dissociation constant (pKa) value can significantly affect the photochemical degradation efficiency. However, the results differ from one study to another, possibly due to the high dependence on the degree of ionization of the model compounds. For instance, in comparison with other pH conditions, at the pH conditions related to the pKa values of difloxacin (4.33 and 9.05), a slower photodegradation rate of this compound was found by Prabhakaran et al [37]. Comparatively, Latch et al. showed that triclosan was rapidly photodegraded at pH values above its pKa [40]. SHA is a hydroxamic acid derivative of salicylic acid, with pKa value of 7.4 for the

hydroxamic acid group and 9.8 for the phenolic hydroxyl group [41]. Interestingly, the photolysis rate of SHA increases with the increase in pH, i.e., with increase in the fraction of a deprotonated form of SHA. These results suggest that hydroxamate form has higher photoreactivity as compared to the molecular form. This observation highlighted that the ionization state of the SHA molecules is one of the key elements to affect its photochemical destruction.

During the UV/H_2O_2 process, increase in the pH from 5.0 to 9.0 lowered the BHA (pKa 8.71) and NOP (pKa 6.10) removal efficiency from 76.22% to 68.16%, and from 57.25% to 44.51%, respectively in 60 min (Fig. 2b-c). Moreover, at pH values of 5.0, 7.0 and 9.0, the corresponding observed $k_{obs,BHA}$ were found to be 0.0242, 0.0193 and 0.0189 min^{-1}, respectively. At the same pH values, $k_{obs,NOP}$ were found to be 0.0146, 0.0108 and 0.0097 min^{-1}, respectively. Actually, the standard redox potential of $HO^{\bullet}$ varies as the pH of the system varies. Specifically, the standard redox potential of $HO^{\bullet}$ in alkaline conditions is approximately 1.9 - 2.0 eV which is lower than that in acidic conditions (2.4 - 2.7 eV) [30]. Moreover, the fraction of HO_2^- (the conjugated base of H_2O_2) increased with the increase in pH and it could react with residual H_2O_2 to scavenge the $HO^{\bullet}$ generated (R S5-S7, Table S4), which may reduce the $HO^{\bullet}$ level that can be produced via UV-activated H_2O_2. Thus, the decrease in the oxidation capacity of $HO^{\bullet}$ and increase in the proportion of HO_2^- in alkaline pH conditions could be responsible for inhibition in the degradation of BHA and NOP.

The influence of pH on UV/PDS system exhibited a reverse trend to that of the UV/H_2O_2 system: with the increase of pH, the removal rate of HAAs increased. For example, during the treatment time, 79.39%, 92.58% and 97.94% degradation of SAH, 84.56%, 91.42% and 99.75% degradation of BHA, and 70.82%, 76.54% and 81.42% degradation of NOP were observed at pH 5.0, 7.0 and 9.0, respectively (Fig. 2d-f).

These results are supported by two mechanisms. First, PDS consumption involved both non-catalytic and acid-catalyzed pathways. Hence, under acidic conditions, PDS will be decomposed in a non-radical reaction to generate less reactive substances such as HSO_4^- and SO_4 instead of $SO_4^{\bullet-}$ (R S8, Table S4) [29]. Second, base-activated PDS activation is enhanced at high pH values (R S9, Table S4) [42]. These factors may cause a change in HAAs degradation in the UV/PDS reaction. A similar phenomenon was reported by Tan et al, who noticed that the k_{obs} of antipyrine degradation by UV/PDS continuously increased from 1.346 h^{-1} at pH 2.5 to 2.005 h^{-1} at pH 11.5 [42]. Undoubtedly, a higher HAA removal rate in alkaline conditions, which is the ambient pH of natural water, is an additional benefit of the utilization of UVA-B/PDS technology for degradation of HAA.

3.3. Role of radicals in the UVA-B/H_2O_2 and UVA-B /PDS reactions

3.3.1 Identification of the main radical species

As elucidated in Fig. 3a, DMPO-$HO^{\bullet}$ and DMPO-$SO_4^{\bullet-}$ signals observed in the ESR spectra are an explicit evidence for the existence of both radicals in the system. To identify the main radical species and quantify their contributions to HAA removal, specific quenching experiments were conducted. Various radicals can be generated during the UV/H_2O_2 or UV/PDS processes, including $HO^{\bullet}$, $SO_4^{\bullet-}$, and other secondary radicals, such as $HO_2^{\bullet}/O_2^{\bullet-}$, $SO_5^{\bullet-}$ (R S3, S10-11, Table S4). HAA destruction via indirect $HO_2^{\bullet}/O_2^{\bullet-}$ (EO $HO2^{\bullet}$ > 1.0, EO $O2^{\bullet-}$ = 0.057 ± 0.01V) or $SO_5^{\bullet-}$ (EO $SO5^{\bullet-}$ = 1.1v) oxidation was disregarded in this study because of their relatively low E^o values [43]. Tert-butanol (TBA) was selected as a scavenger for $HO^{\bullet}$ due to the fact that its reaction with $HO^{\bullet}$ (R S12; Table S4) is approximately 3 orders of magnitude faster than the one with $SO_4^{\bullet-}$ (R S13; Table S4). As it has high rate constants with both $HO^{\bullet}$

(R S14; Table S4) and $SO_4^{\bullet-}$ (R S15; Table S3), ethanol (EtOH) was used to effectively scavenge both of these radicals.

Effect of radical scavengers (TBA and EtOH at different concentrations) on the removal of HAAs in UVA-B/AOP is presented in Fig. 3. As expected, during the UV/H_2O_2/TBA and UV/H_2O_2/EtOH processes (Fig. 3b-c), both, BHA and NOP degradation were significantly suppressed and the k_{obs} was reduced by more than 90%. Considering the fact that direct photolysis of BHA and NOP was negligible, degradation of these compounds should be solely attributed to the $HO^{\bullet}$-mediated oxidation. In general, the $SO_4^{\bullet-}$ can react with H_2O or OH^- (R S16-17, Table S4) leading to the generation of $HO^{\bullet}$ in the UV/PDS system. As elucidated in Fig. 3e-f, with the increase in concentration of TBA from 100 to 300 mM, the degradation processes of BHA and NOP were inhibited by 32.99% - 50.64% and 17.87% - 31.06%, respectively. These results clearly proved the presence of $HO^{\bullet}$ in UV/PDS system for degradation of HAAs. On the contrary, even at a relatively low concentration of EtOH, the removal efficiencies of BHA and NOP were reduced to close to zero. The inhibition effect of EtOH is stronger than that of TBA which demonstrated that $HO^{\bullet}$ and $SO_4^{\bullet-}$ were predominant active species for BHA and NOP removal in the systems investigated. The degradation of SHA in the UV/PDS reaction was inhibited by only 2.09% - 7.88% in the presence of 100 - 300 mM TBA, while the degradation rate of SHA was almost identical to the UVA-B photolysis alone in the presence of 100 - 300 mM EtOH (Fig. 3d). These results imply that the indirect photodegradation of SHA was highly depended on $SO_4^{\bullet-}$.

3.3.2. The contribution of radicals to the degradation of SHA, BHA and NOP in the UVA-B/PDS system

Fig. 4 illustrates the contribution of radicals to the removal rates of HAAs during the UVA-B/PDS processes at each of the pH levels used. The details on the calculation of the contributions of UVA-B photolysis, $HO^{\bullet}$, and $SO_4^{\bullet-}$ on HAAs removal are provided in Text S4. At pH 5.0, 7.0 and 9.0, the contributions of $SO_4^{\bullet-}$ to degradation of SHA were calculated to be 6.96%, 24.27% and 31.85%, respectively. These results imply that the degradation of SHA via the $SO_4^{\bullet-}$-mediated oxidation is becoming more prominent with increase in pH. Even so, direct photolysis was still the dominant part of k_{obs} (more than 65%), demonstrating that the SHA destruction was primarily owned to the UVA-B photolysis. At the pH values used in this study (5.0, 7.0, and 9.0), the contributions of $SO_4^{\bullet-}$ to degradation of BHA were 92.56%, 90.56%, 95.33%, and to degradation of NOP were 85.78%, 91.91%, 92.01%, respectively. Taken as a whole, no matter how their contributions changed, the degradation of BHA and NOP in the UVA-B/PDS system were always predominantly driven by $SO_4^{\bullet-}$, whereas $HO^{\bullet}$ played a much less important role. Similar trends were reported by Hoang et al, who revealed that in the UV/PDS degradation of methyl orange, $SO_4^{\bullet-}$ was the main radical while the contribution of $HO^{\bullet}$ was much lower [44].

3.3.3 Second-order rate constants of $HO^{\bullet}$ and $SO_4^{\bullet-}$ reacting with three HAAs

The second-order rate constants of the reactions of HAAs with $HO^{\bullet}$ and $SO_4^{\bullet-}$ achieved by using a competition kinetics approach (Text S4). The results revealed a different reactivity of the pollutants investigated in this work. As explained in the Section 3.2.1, HAAs were mainly removed in the reactions mediated by $HO^{\bullet}$ and $SO_4^{\bullet-}$. The second-order rate constants of BHA and NOP with $HO^{\bullet}$ were calculated to be 5.22×10^9 $M^{-1}\cdot s^{-1}$ and 4.16×10^9 $M^{-1}\cdot s^{-1}$ (Fig. 5a). The second-order rate constants of SHA (the contribution of the direct SHA photolysis has been deducted), BHA and NOP with $SO_4^{\bullet-}$ were calculated to be 4.83×10^9 $M^{-1}\cdot s^{-1}$, 7.22×10^9 $M^{-1}\cdot s^{-1}$ and $1.19 \times$

10^9 $M^{-1}\cdot s^{-1}$ (Fig. 5b). It is found that the rate constant of the reaction between NOP and $SO_4^{\bullet-}$ was approximately four times lower than the one between SHA and $SO_4^{\bullet-}$ and approximately six times lower than the one between BHA and $SO_4^{\bullet-}$. Considering the electrophilic nature of $SO_4^{\bullet-}$, aromatic compounds with a stronger electron-donating substituent are prone to react with $SO_4^{\bullet-}$ [25]. This fact can explain the lower reactivity of NOP than SHA and BHA since -NHOH is a stronger electron-donating substituent than -OH on the heterocycle. Moreover, the second-order rate constants between each of the HAAs investigated and $HO^{\bullet}$ or $SO_4^{\bullet-}$ have the same order of magnitude and they are close to the diffusion control limit. These results indicate that these HAAs are vulnerable to the electrophilic attacks by both, $HO^{\bullet}$ and $SO_4^{\bullet-}$ [38].

3.4. The influence of NOM and water matrix

3.4.1 The influence of NOM and inorganic anion

The influences of NOM and Cl^-, HCO_3^- and NO_3^-, four prevalent natural water constituents, on the removal of SHA, BHA and NOP by the UV/AOP system were systematically investigated. Studying the reactivity of the water matrixes towards radicals will contribute to gain insights into the destruction of HAAs by AOPs in natural and engineered water systems.

The presence of HA that served as a surrogate of the aquatic NOM, considerably slowed down the removal rate of three HAAs (Fig. 6). The inhibitory effect of HA further exacerbated with increase in its concentration. In particular, in the presence of 10 mgC L^{-1} HA, direct photolysis rate of SHA was reduced by 71.43%. The reaction rates of BHA and NOP degradation in UV/H_2O_2 system decreased by 53.89% and 50.92%, respectively, while the reaction rates of SHA, BHA and NOP removal in UV/PDS system decreased by more than 75%. The combination of light screening effect and radical scavenging effect are the primary causes of this phenomenon. First,

NOM can screen a fraction of light due to an inner filter effect, which can hinder the photochemical generation of reactive radicals from the oxidant or inhibit the direct photolysis of SHA. Second, HA can competitively react with $HO^{\bullet}$ and $SO_4^{\bullet-}$ (R S18-19, Table S4), making them less available for reaction with HAAs [38, 45]. It is noteworthy that the inhibitory effect of high levels of HA (10 mgC L^{-1}) is observed to be more pronounced in the $SO_4^{\bullet-}$-mediated oxidation than in the $HO^{\bullet}$-mediated oxidation. This result can be ascribed to the phenolic and carboxylic moieties in the HA molecule. These groups are vulnerable to $SO_4^{\bullet-}$ attack via electron transfer and decarboxylation mechanisms, which can further reduce the amount of $SO_4^{\bullet-}$ available for reaction with the target contaminants [38].

The inhibitory impact of Cl^- on the $HO^{\bullet}$ and $SO_4^{\bullet-}$-mediated oxidation of pollutants has been extensively documented in the literature, and examples included isoproturon [29], amoxicillin [39], oxytetracycline [46]. As illustrated in Fig 6a-c, the presence of Cl^- in the system during the UV/AOPs process suppressed k_{obs} of the HAAs to different extent. This effect was probably caused by reaction of Cl^- with $HO^{\bullet}$ and $SO_4^{\bullet-}$ that might produce lower reactive radicals at a high reaction rate ($ClOH^{\bullet-}$, $Cl^{\bullet}$ and $Cl_2^{\bullet-}$, R S20-26, Table S4) [25, 29]. However, it was observed that the inhibition in the UV/PDS system (0.43 - 30.10% reduction) was obviously higher than that in the UV/H_2O_2 system (0 - 7.41% reduction). Although Cl^- can scavenge $HO^{\bullet}$ at a relative high reaction rate (R S20, Table S4) [25], there is also a rapid reverse reaction, and the net result is only a partial consumption of $HO^{\bullet}$ by Cl^-.

Many studies reported that the presence of CO_3^{2-} and HCO_3^- can not only change the alkalinity of natural waters but they are also able to compete with target compounds to react with radicals during various AOPs. In general, HCO_3^- plays a negative role in AOPs owing to the scavenging effect on radicals (R S27-30, Table

S4). Unexpectedly, a positive impact of HCO_3^- on HAAs degradation was discovered in this study. Chen et al. also observed the promoting effect of HCO_3^- toward propranolol degradation during the UV/PDS process [47]. The promotion of HCO_3^- might be explained by two related aspects. First, the occurrence of HCO_3^- can change the alkalinity of the solution. The pH of the reaction mixture varied from 7.0 to 7.6 when the concentration of HCO_3^- increased from 1 mM to 10 mM, causing the pH effect as described in Section 3.2. This fact can largely interpreted why k_{obs} of SHA barely changed in the presence of 0.1-1 mM HCO_3^- while k_{obs} of SHA increased by 27.86% (UV only system), and by 36.94% (UV/PDS system) in the presence of 10 mM HCO_3^-. Second, the k_{obs} increased in the UV/H_2O_2 system within low concentrations range (0.1 - 1 mM; pH 7.0 - 7.1) when the solution was introduced with HCO_3^-, although the rate should have remained stable or dropped, if only taking the changes in alkalinity into consideration. This indicates that the reaction between secondary radicals $CO_3^{\bullet-}$ and HAA might have been involved. Although the redox potential of $CO_3^{\bullet-}$ (1.78 V, pH 7) is lower than the one of $HO^\bullet$ and $SO_4^{\bullet-}$, they are highly selective for electron-rich compounds, for example, nitrogen- and sulfur-containing substrates and aromatic compounds [48]. Due to the existence of a lone pair of electrons on the hydroxamic acid group, HAAs belong to the electron-rich compounds. Therefore, in this work, the reactions of $CO_3^{\bullet-}$ with HAAs that contain an electron-rich hydroxamic acid moiety compensated the loss of $HO^\bullet$ and $SO_4^{\bullet-}$ and even enhanced the removal efficiency of the process. Hence, HCO_3^- might play a major role in the practical application by promoting HAAs degradation and should not strictly be regarded as a radical scavenger.

The results are presented in Fig. 6 from which it can be seen that the removal of three selected HAAs in the UV/AOP systems was affected by addition of NO_3^- to

varying degrees. Theoretically, the absorption spectra of NO_3^- in solution are dominated by weak bands of $n \rightarrow \pi^*$ transitions of non-bonding n-electrons at approximately 300 nm and 360 nm. They can absorb some radiation within the UVA-B region (280 - 400 nm), thereby producing (via direct photolysis of NO_3^-, R S31-32, Table S4) additional $HO^\bullet$ at a low quantum yield [49-50]. As depicted in Fig. S1, the strong absorption peak of NO_3^- at 301 nm also supports this possibility. Previous work by Peng et al reported that the presence of NO_3^- could enhance the removal of diclofenac by UV/peroxymonosulfate treatment because NO_3^- can be activated to generate $HO^\bullet$ under UV irradiation [51]. In the UV/PDS system, the k_{obs} of NOP in the presence of 0.1 - 10 mg/L NO_3^- increased by 6.81%, 8.51% and 24.25%, respectively, suggesting that the k_{obs} increased with increasing concentration of NO_3^-. At the same time, the k_{obs} of BHA increased by 11.48%, 15.05% and 2.29%, respectively and the highest k_{obs} was obtained at 1.0 mM NO_3^-. The reason for this difference may be that in the presence of high levels of NO_3^-, the excessive NO_3^- might compete with PDS for incident UV. This might reduce the production of $SO_4^{\bullet-}$ and, accordingly, decrease the k_{obs} of BHA degradation. On the contrary, the high reactivity of the $HO^\bullet$ toward NOP compensated for the decreased contributions of $SO_4^{\bullet-}$ and maintained a higher k_{obs} for NOP. Additionally, the addition of 0.1 - 10 mM NO_3^- lowered the k_{obs} of SHA by 0.46% - 14.53% in the UV/PDS system, which is likely ascribed to the ability of NO_3^- to compete with PDS for UVA-B photons and to generate low-reactivity $HO^\bullet$ with SHA. It is also noted that NO_3^- can scavenge both $HO^\bullet$ and $SO_4^{\bullet-}$ according to R S33-34 (Table S4). However, NO_3^- exhibits insignificant impact in both systems, due to its low reaction rates with both, $HO^\bullet$ and $SO_4^{\bullet-}$.

3.4.2 The influence of metal cations

Metal ions are widely distributed in mineral processing wastewater. Several transition metals (including Fe^{2+}, Fe^{3+}, Cu^{2+} and Mn^{2+}) were investigated for their effects on degradation of three HAAs in the UVA-B/AOP system. As presented in Fig. 7b-c, the degradation of BHA and NOP enhanced with increase Fe^{2+} concentration in both, UV/H_2O_2 and UV/PDS systems. It has been well established that common transition metals are able to activate H_2O_2 or PDS to generate more radical species. Furthermore, it has been observed that BHA and NOP are eliminated much more efficiently in the UV/H_2O_2 system than in the UV/PDS system. This can be explained by the fact that the activation rate of H_2O_2 (70 M^{-1} s^{-1}) by Fe^{2+} is higher than the activation rate of PDS (27 M^{-1} s^{-1}, R S35-36, Table S4). In fact, excessive Fe^{2+} were reported to potentially lead to undesired competition reactions which rapidly scavenge radicals (R S37-38, Table S4). This phenomenon was not found in this study, possibly because the Fe^{2+} concentration was below the inhibition threshold.

Fe^{3+} can act as a catalysts to generate $HO^{\bullet}$ in UV/ Fe^{3+}/H_2O_2 system via two pathways: (1) a classical Fenton-type reaction for Fe^{3+}/H_2O_2 system (R S35, S39-41, Table S4) [46]. However, this reaction is sensitive in a relatively narrow pH range of 2.5 - 4.0. (2) photosensitizing effect of $FeOH^{2+}$ provides in situ Fe^{2+} for the Fenton reaction (R S42, Table S4). Nevertheless, $FeOH^{2+}$ mainly exist in a pH range of 2.5 - 5.0. Additional $HO^{\bullet}$ can barely be produced in the present UV/Fe^{3+}/H_2O_2 system because the solution pH is 7 and Fe^{3+} exist primarily as $Fe(OH)^{2+}$, $Fe(OH)_3$ and $FePO_4$. This can explain why the presence of Fe^{3+} ions did not efficiently enhance degradation of BHA and NOP during the UV/H_2O_2 process. Similar phenomena have been observed in the UV/PDS system.

Unlike Fe^{3+}, Cu^{2+} ions were capable of activating H_2O_2 or PDS in a broader pH range. As expected, the presence of Cu^{2+} also enhanced the removal of HAAs in

UV/H_2O_2 and UV/PDS systems. Differently, the kobs of HAAs in the presence of Cu^{2+} followed a bell-shaped trend with increase their concentrations. This phenomenon can be caused by the following reasons: First, higher Cu^{2+} concentration reduces the UV transmittance effect, and then interfere with the formation of radical species. At the same time, Cu^{2+} slows down the reaction of UV photons with the precursors of the radical species [52-53]. Second, one part of $HO^{\bullet}$ and $SO_4^{\bullet-}$ was scavenged by the excess Cu^{2+}. It should be noted that the photodegradation of SHA was inhibited when high levels of $Fe^{2+}/Fe^{3+}/Cu^{2+}$ were added to the solution. Possible explanation for this observation might be the fact that: SHA easily forms chromatic complexes with transition metal ions which can reduce the UV transmittance effect.

Regarding the influence of Mn^{2+}, no difference in HAAs degradation was observed with Mn^{2+} concentration ranging from 0 to 0.1 mM in UV/AOP systems. Anipsitakis and Dionysiou have proved that Mn^{2+} was an ineffective activator for H_2O_2 and PDS [54]. When the concentration of Mn^{2+} increases to 1.0 mM, the degradation of HAAs were inhibited during both UV/H_2O_2 and UV/PDS processes, probably due to excess Mn^{2+} compete with HAAs for reactive radicals.

3.5. Performance of the UVA-B/AOP processes and radicals' consumption distributions in real wastewaters

To evaluate the practical performance of the UV/AOP process, HAAs were used as model target contaminants and two real waters (WE and SW) from a non-ferrous smelting assembly were used as a background. The sources and the major water quality parameters of the real water samples are listed in Table S5. Fig. 8a presents that the direct photolysis rate of SHA in WE is slightly inhibited compared to that in the Milli-Q water, while it is reduced by 11.73% in SW. In the $HO^{\bullet}$-mediated AOP process, the $k_{obs,BHA}$ in WE and SW were 17.09% and 38.34% lower than that in the

Milli-Q water (Fig. 8b). The $k_{obs,NOP}$ in WE and SW were 21.29% and 27.78% lower than that in the Milli-Q water (Fig. 8c). On the other hand, in the $SO_4^{\bullet-}$-mediated AOP process, the k_{obs} of SHA and NOP decreased by 12.75%, and 14.04% in WE, and 17.31%, and 22.13% in SW, respectively. Unexpectedly, the k_{obs} of BHA slightly increased by 6.63%, and 3.82% in two real waters.

These results can be further explained by the discussion of the consumption distributions of $HO^{\bullet}$ and $SO_4^{\bullet-}$ in two water samples. The calculation details are given by Eq. (1) [55]:

$$R_{a,b} = \frac{k_{a,b}C_b}{\sum_{b=1}^{b} k_{a,b}C_b} \times 100\% \qquad (1)$$

where $R_{a,b}$ and $k_{a,b}$ are the radicals consumption fraction (%) and second-order rate constant ($M^{-1}\cdot s^{-1}$ or $M_C^{-1}\cdot s^{-1}$) of a radical (a) with a specific water matrix (b), respectively, and C_b is the concentration (M or M_C) of b.

The calculated results are plotted in Fig. 8d-f. It is obvious that the presence of NO_3^- and HCO_3^- did not noticeably contribute to the consumption of $HO^{\bullet}$ or $SO_4^{\bullet-}$ in two actual waters owe to either low reactivity or low concentration (< 0.01 mM). In the UV/H_2O_2 process, 15.82% - 18.17% and 26.76% - 29.61% of $HO^{\bullet}$ reacted with Cl^-, in WE and SW, respectively. However, since the reactions are reversible, the real fraction of $HO^{\bullet}$ consumed by Cl^- is probably much lower than the value calculated in this work. Dissolved organic carbon (DOC) scavenged 23.77% - 27.15% and 27.99% - 30.98% of $HO^{\bullet}$, in WE and SW, respectively, suggesting that the DOC contained in the real water samples is the key factor to inhibit the removal of target pollutants during the UV/H_2O_2 process. Nevertheless, there was a remarkable difference in the consumption distributions of $HO^{\bullet}$ and $SO_4^{\bullet-}$. Fig. 8e exhibits that BHA (95.18% - 97.37%) was the main component responsible for $SO_4^{\bullet-}$ consumption. DOC and Cl^-

scavenged less than 5% of the $SO_4^{\bullet-}$. In comparison, 84.06% and 73.70% of $SO_4^{\bullet-}$ was consumed by NOP in the WE and SW, respectively. The percentages of $SO_4^{\bullet-}$ scavenged by Cl^- and DOC are 6.87% - 13.64% and 8.86% - 12.32%, respectively, which may interpret why a larger decrease was found in the k_{obs} of NOP, but not in BHA. These phenomenon show that NOP degradation during UV/PDS process in real water was much more inhibited by water matrix than degradation of BHA. It should be noted that more than 90% of $SO_4^{\bullet-}$ in UV/PDS systems was consumed by SHA, but the k_{obs} of SHA in WE and SW were still 12.75% - 17.31% lower than in the Milli-Q water. This can possibly be due to the shielding effect of DOM that weakens SHA removal via direct photolysis. Even so, relatively satisfactory degradation of the HAAs investigated can be achieved by the UV/PDS process in real wastewaters.

3.6. Proposed degradation pathway and mechanism

As indicated above, the efficient degradation of hydroxamic acids was achieved in the UVA-B/AOP system. Nevertheless, to further understand the practical application potential of this technology, prior evaluation of the formation of TPs is necessary. Fukui function has been previously used in many studies to predict the active sites on organic molecules [56-57]. Generally, in the compound, the atom with the higher f^0 is more vulnerable to a radical attack, while the atom with the higher f^- is more vulnerable to an electrophilic attack [56-57]. The condensed Fukui function of HAAs with the calculated values listed in Table S6. The degradation pathways of HAAs were proposed by combining the detected intermediates (Table S7) with the calculated Fukui index. For f^0, the highest values occurred at C1, C2, C3 and O7 in the molecule of SHA; at C2, N8, O9 and O10 in the molecule of BHA; at C1, C2, N8, O10 and O11 in the molecule of NOP, depicting that the radical attacks were supposed to occur around those atoms (Table S6).

Based on the identified TP structures and Fukui index, detailed transformation mechanism and pathways of HAAs in the UVA-B/AOP system are preliminarily proposed and exhibited in Fig. 9. Initially, owing to the higher value of f^0 and the highest values of f^-, the reactive sites N8 of BHA and N8 of NOP as the active sites for the electrophilic attack were attacked by radical and formed amidated products (TP9 and TP15). However, SHA also generated amides although the f^0 and f^- values of N10 were lower than those of other atoms, suggesting that TP1 may be formed by direct photolysis rather than by free radical attack. Agnieszka et al. have clarified the photodegradation mechanism of SHA (Scheme 1) [58]: under UV radiation, SHA forms a compound with a structure between a nitrene and an oxazirene. This reaction proceeds by hydrogen elimination from the hydroxamic nitrogen and detachment of a hydroxyl group, and finally by rearrangement of the rest of the molecule to o-hydroxyphenylisocyanate. Next, o-hydroxyphenylisocyanate picks up two hydrogens from the solution to produce salicylamide. Subsequently, these amidated products are further hydrolyzed into the corresponding carboxylic acids. According to the described reaction sequence, it can be reasonably speculated that the formation of the corresponding carboxylic acid from HAA is considered as the initial degradation reaction step, which might be generalized to the degradation pathway of HAA collectors with more complex structures.

Hydroxylation is a significant reaction pathway induced by $HO^{\bullet}$ or $SO_4^{\bullet-}$ attack, and the aromatic ring may be a preferable hydroxylation reaction site, but the reaction mechanism is discriminating. The reaction mechanism between $HO^{\bullet}$ and the aromatic ring is electrophilic attack, that is, hydrogen abstraction and/or hydroxyl addition to unsaturated carbon [59-60]. However, due to its electrophilic property, $SO_4^{\bullet-}$ preferentially undergoes electron transfer reactions. In this process, a direct electron

transfer from an aromatic ring to $SO_4^{\bullet-}$ produces a short-lived sulfate radical adduct. This adduct is able to undergo the elimination of a sulfate anion and form a radical cation. Finally, the radical cation generates -OH adducts by hydrolysis [59, 60-61]. Based on the described mechanism, similar hydroxylation TPs, such as TP1 and TP5 (in the degradation pathway of BHA), TP2, TP3, TP10, TP12, TP14 and TP16, could be generated through the direct attack of different radicals on the respective positions of the aromatic ring. This is consistent with the aforementioned prediction of the Fukui index, which estimates that these sites with larger f^0 values are susceptible to radical attack.

In the transformation pathway of BHA, the formation of TP5 and TP12 had two potential pathways: one is a hydroxylation of TP11 on the aromatic ring and the other one is a hydrolysis of the amine groups in TP1 and TP10. Regarding TP5 with monohydroxy structure, the hydroxyl group can act as a strong electron donor, which makes the ortho/para positions more electron-rich [62]. Theoretically, oxidants tend to attack the ortho and para positions of the aromatic ring, with the production of multi-hydroxyl (two to three -OH groups) intermediates, such as 2,3-dihydroxybenzoic acid (TP4) or 2,5-dihydroxybenzoic acid (TP6). Nevertheless, they were not detected in this study, which could be possibly due to lower yield, rapid transformation, or simply absence of formation. A similar phenomenon of a missing intermediate was also reported by Ding et al [63]. Even so, it seems to be one of the possible TPs if their generation really follows the pathway of reaction. At the end of the reaction, mass balance calculations also confirmed the presence of some unidentified TPs (Table S8).

In the NOP oxidation system, TP5 and TP11 were also identified as the products of TP17, and they were generated first by attack on the α-C of carboxylic group, followed by a decarboxylation mechanism. Subsequently, further decarboxylation

from TP11 results in the formation of TP13, which is consistent with the recent study on degradation pathway of dimethyl phthalate proposed by other researchers [63]. As shown in Scheme 2, the TP5 would be deprotonated to produce 2-hydroxybenzoate as an intermediate whose carboxylate group might be attacked and then converted to TP7 or completely eliminated to generate TP8 [64]. Furthermore, TP7 was also likely to be formed in a reaction of an aromatic substitution in TP8 which preferentially directs -OH addition to its electron rich ortho site [65]. Finally, all these hydroxylation and decarboxylation products can be further oxidized, leading to the breakage of the benzene ring, and production of a series of short-chain aliphatic acid (2-butenoic acid, butyric acid, etc.).

Evaluation of the double bond equivalent (DBE) of the transformation products is helpful for structure elucidation, and the results are presented in Table S7. All transformation products had DBE values distributed between 4 and 7, indicating which of these TPs might have a single aromatic ring (the benzene ring shows DBE values of 4). Those of TPs with DBE values of 5 and 6 are likely aromatic rings with a double bond in the side chain. For TPs having 8 carbon atoms and DBE = 7, they are more likely to have a N-heterocyclic structure. Generally, epoxy, acyl, carbanyl or carboxy groups can induce a unit increase in DBE value per compound while ether and hydroxy groups make no contribution to the DBE values [66]. This means that decarboxylic reaction process results in a reduction of the DBE value by 1 for TPs, while the hydroxyl addition on the aromatic ring cannot change their DBE values. The products with DBE = 1 or 2 do not have any aromatic structures and could be assigned to short-chain aliphatic acids which are generated by the breakage of the benzene ring. Overall, proposed structures of TPs were further proved via the DBE values.

3.7. Mineralization of HAA

TOC is used as a measure of mineralization of target organic pollutants. As it can be observed in Fig. 10, direct photolysis is sufficient for a complete destruction of SHA during UV process only, but the level of SHA mineralization in terms of TOC removal is very low. This could be ascribed to the fact that TPs of SHA are not susceptible to direct photolysis. By contrast, 6.75% TOC was removed after 20 min of irradiation and reached 21.67% after 60 min of irradiation in the UV/PDS system. For the other two HAAs, i.e., BHA and NOP, the TOC removal was 13.33% and 8.73% in UV/H_2O_2 system, while the TOC removal in UV/PDS system was 18.14% and 14.93%, respectively, after 60 min of the reaction time. These results indicate that UV/PDS process is more efficient in degradation of BHA, NOP and their TPs, which leads to the higher mineralization as compared to the UV/H_2O_2 process. Furthermore, a large fraction of HAAs was transformed into their TPs without a complete mineralization, possibly because production of radicals-resistant TPs relative to HAAs. Accordingly, a longer treatment time is probably needed for further mineralization. Fig. S2 also shows the consumption of H_2O_2 and PDS during the degradation of HAAs, which was relatively a slow process. There were only around 13.13-14.58% H_2O_2 and 19.61-20.86% consumption in 60 min. Although sufficient oxidants can induce further decomposition of TPs, the oxidant utilization efficiency may need to be enhancement, which was significant for a mineralization.

3.8. Ecotoxicity evaluation

The overall toxicity of the HAAs treated by UV/AOP were evaluated with a luminescence inhibition assay using *Vibrio fischeri*. The L/L0 represents the ratio of a sample luminescence with the initial luminescence (i.e., before treatment at t = 0). A lower L/L0 value indicates a higher acute toxicity. The ecotoxicities of three HAAs and individual TP were also predicted using the ECOSAR program. Table S9 shows

that the HAAs and their TPs revealed different ecotoxicity levels for fish, daphnia, and green algae.

As depicted Fig. 11, in the case of BHA and NOP, similar tendencies of toxicity could be observed during both the UV/H_2O_2 and UV/PDS processes. Specifically, the bioluminescence inhibition in *Vibrio fischeri* at first increased, and then decreased with the progress of the reaction. Based on the eco-toxicity estimation performed using ECOSAR, except for TP2 and TP3, the intermediates with amide structure produced in UV/AOP exhibited higher acute toxicity for all tested aquatic organisms compared to the parent pollutants. Although with some exceptions, it is observed that the introduction of -OH groups to the precursor resulted in an enhanced toxicity due to the increased reactivity of these TPs [29]. This implys that the acute toxicity increase during HAAs removal during the UV/AOP reaction processes may result from the formation of these aminated and hydroxylated products. A similar phenomenon was found when Zhang evaluated the acute toxicity of trimethoprim and sulfamethoxazole and their TPs by UV/AOP treatment [67]. The overall toxicity continually attenuated during the subsequent reaction process owe to the further decomposition of the toxic TPs. Furthermore, the carboxylic acid products such as TP5, TP11 and TP17, which generally showed lower toxicity than the parent molecules, may also lead to the change of the total toxicity of the reaction mixture during the degradation processes. The gradual mineralization of TPs may also be an important reason for the continuous detoxification of the reaction solution. In the UV only system, the luminescence of the SHA samples decreased to 85% of the initial luminescence, suggesting that TPs by direct photolysis slightly increased the toxicity of the system. The result still had a certain significance, indicatting that UVA-B direct photolysis can rapidly degrade SHA, but did not cause its mineralization and

detoxification. SHA samples treated by UV/PDS retained a higher toxicity compared to the UV photolysis, maybe because highly toxic intermediates, such as TP8 and TP13, were generated during degradation and their mineralization was not efficient enough during 20 min. Some intermediates presented a different behavior. For instance, TP7 was observed to be more toxic toward fish and green algae, but less toxic toward daphnia than SHA. This phenomenon illustrates that certain precautions during UV/AOP processes must be considered to prevent the formation of intermediates that pose an excessive ecological risks. Additionally, the combined pollution effects of HAAs and heavy metals is an environmental problem that cannot be ignored. In this regard, the evaluation of the overall toxicity of the system deserves further discussion.

3.9. Economic comparison of UVA-B/H_2O_2 and UVA-B/PDS processes

Since the UV-based AOPs are typically electric-energy intensive, electrical energy may account for a major fraction of the operating costs. In order to further evaluate the practicability of UVA/AOPs for HAAs degradation, an economic analysis using the EE/O concept was applied and the electrical energy of the UV lamp and the consumption of oxidants were considered in the EE/O evaluation [68]. A detailed demonstration of the calculation of the EE/O is provided in SI Text S5. The higher the EE/O implies lower process efficiency and higher operating cost. As shown in Table 1, despite direct photolysis accounted for the majority of the destruction of SHA in both UV only and UV/PDS processes, UV/PDS process is more cost-efficient than UV process only, indicating that the addition of PDS might have helped to lower the EE/O. For the BHA and NOP which are degraded mainly by the reactive species, the energy consumption of UV/PDS process is lower than the energy consumption of UV/H_2O_2 process with the same oxidant concentration and UV fluence. This depends

on the higher degradation rate of BHA and NOP in UV/PDS process. Comprehensive evaluation of the influence of degradation efficiency, EE/O and TOC on UVA-B/AOP systems, revealed that UVA-B/PDS process is more efficient and economical for HAAs removal. Consequently, PDS could be applied as an alternative oxidant in wastewater containing HAAs treatment.

3.10. Comparison with other AOPs

Table S10 exhibits the main characteristics of the processes used for the removal of typical floatation reagents by other AOPs and their results are compared with the current work. It was found that all the AOPs have both, advantages and disadvantages. Efficiency is a pervasive advantage of these AOPs. O_3 based AOPs have many advantages for mineral processing wastewater treatment, but the cost of O_3 production is a major limitation for their large-scale application. Among the heterogeneous catalysts-based AOPs, although synthetic catalysts may be costly, this imperfection can be compensated by other catalyst properties such as the possibility to recover and reuse them. However, these synthesized catalysts are currently limited to laboratory-scale applications, and their further application in industrial-scale wastewater treatment remains a key challenge. UV-based AOP require a neutral or a basic solution and therefore, they are simpler to apply and relatively cheaper in comparison to other AOPs. Some disadvantages that have been observed in the current work, such as low mineralization rate, and residual sulfate ions, should be considered in further research.

4. Conclusion

This work reveals that UVA-B/AOP effectively eliminated three typical hydroxamic acids collectors. The following conclusions can be obtained: Direct photolysis makes predominant contribution to SHA degradation in UV/H_2O_2 and

UV/PDS system. However, direct UVA-B irradiation showed negligible impact on photolysis of BHA and NOP, while the addition of oxidant significantly enhanced the removal efficiency of BHA and NOP. In the acidic medium, $HO^{\bullet}$ was more efficient for HAA removal, while $SO_4^{\bullet-}$ was more efficient for HAA removal in the alkaline medium. Using a competition reaction kinetics approach, the second-order rate constants for reactions of $HO^{\bullet}$ and $SO_4^{\bullet-}$ with SHA, BHA and NOP, were determined to be $(4.16 - 5.22) \times 10^9$ $M^{-1} \cdot s^{-1}$ and $(1.19 - 7.22) \times 10^9$ $M^{-1} \cdot s^{-1}$, respectively. Furthermore, the addition of HA and Cl^- inhibited HAAs destruction to different degrees, while a promotion effect was observed in the presence of HCO_3^-, Fe^{2+} and Cu^{2+}. However, NO_3^- exhibited inconsistent influences on the HAAs degradation, which depended on the target pollutant. Combined with the intermediates identified and DFT, it was concluded that degradation of HAAs investigated first produced corresponding amide products, and then proceeded primarily via hydrolysis, hydroxylation, decarboxylation and ring opening, from which possible degradation pathways were proposed. Toxicity evaluation suggested that some TPs with higher acute toxicities were generated during HAAs degradation processes. It was presumed that their further decomposition might reduce the overall toxicity of system.

In terms of removal efficiencies in the oxidation process, the UVA-B/PDS system can be a better alternative for HAAs removal in wastewater, compared to the UVA-B/H_2O_2 system. Overall, these results show that UVA-B/AOP is a promising technology to remove HAAs in the actual engineering application. Moreover, in order to comprehensively assess the performance of UVA-B/H_2O_2 and UVA-B/PDS systems in degradation of HAAs, and to minimize the knowledge gaps between a simulated wastewater and a mineral processing wastewater, a further study ought to be considered to assess a combined pollution system of HAAs and heavy metals.

Acknowledgements

This work has been supported partly by grants received from the Major National R & D Projects for Chinese Ministry of Science and Technology (2019YFC1803500), National Science Foundation of China (41720104007), the 111 Project (B21017) as well as by 2021 Graduate Innovation Fund Project of China University of Geosciences, Beijing (YB2021YC016). This research was also partially supported by the Ministry of Education, Science and Technological Development of the Republic of Serbia (Grant No. 451-03-68/2022-14/200026) and by the International Joint Scientific and Technical Collaboration between the People's Republic of China and the Republic of Serbia as part of the Project Number 4-18.

References

[1] K. A. Natarajan and M. R. Sabari Prakasan, Biodegradation of sodium isopropyl xanthate by Paenibacillus polymyxa and Pseudomonas putida, Miner. Metall. Process. 30 (2013) 226-232.
[2] D. M. Araujo, M. I. Yoshida, J. A. Takahashi, C. F. Carvalho, F. Stapelfeldt, Biodegradation studies on fatty amines used for reverse flotation of iron ore, Int. Biodeterior. Biodegrad. 64 (2010) 151-155.
[3] X. Zhu, J. Yao, F. Wang, Z. Yuan, J. Liu, G. Jordan, T. Š. Knudsen, J. Avdalović, Combined effects of antimony and sodium diethyldithiocarbamate on soil microbial activity and speciation change of heavy metals. Implications for contaminated lands hazardous material pollution in nonferrous metal mining areas. J. Hazard. Mater. 349 (2018) 160-167.
[4] M. Li, H. Zhong, Z. He, L. Hu, W. Sun, P. Loganathan, D. Xiong, Degradation of various thiol collectors in simulated and real mineral processing wastewater of sulfide ore in heterogeneous modified manganese slag/PMS system, Chem. Eng. J. 413 (2021) 127478.
[5] J. Kang, W. Sun, Y. Hu, Z. Gao, R. Liu, Q. Zhang, H. Liu, X. Meng, The utilization of waste by-products for removing silicate from mineral processing wastewater via chemical precipitation. Water Res. 125 (2017) 318-324.
[6] H. Han, Y. Hu, W. Sun, X. Li, C. Cao, R. Liu, T. Yue, X. Meng, Y. Guo, J. Wang, Z. Gao, P. Chen, W. Huang, J. Liu, J. Xie, Y. Chen, Fatty acid flotation versus BHA flotation of tungsten minerals and their performance in flotation practice, Int. J. Miner. Process. 159 (2017) 22-29.
[7] A. Jordens, P. C. Ying, K. E. Waters, A review of the beneficiation of rare earth element bearing minerals, Miner. Eng. 41 (2013) 97-114.
[8] G. B. Abaka-Wood, J. Addai-Mensah, W. Skinner, A study of selective flotation recovery of rare earth oxides from hematite and quartz using hydroxamic acid as a collector, Adv. Powder Technol. 29 (2018) 1886-1899.
[9] C. Marion, A. Jordens, R. Li, M. Rudolph, K. E.Waters, An evaluation of hydroxamate collectors for malachite flotation, Sep. Purif. Technol. 183 (2017) 258-269.
[10] X. Luo, J. Wang, C. Wang, S. Zhu, Z. Li, X. Tang, M. Wu, Degradation and mineralization of benzohydroxamic acid by synthesized mesoporous La/TiO_2, Int J Environ Res Public Health. 13 (2016) 997.
[11] M. Araceli, E. Álvarez, A. Uribe-Salas, F. Alonso, Flotation studies of galena (PbS), cerussite ($PbCO_3$) and anglesite ($PbSO_4$) with hydroxamic acids as collectors, Miner. Eng. 155 (2020) 106456.
[12] R. Natarajan and I. Nirdosh, New collectors for sphalerite flotation, Int. J. Miner. Process. 79 (2006) 141-148.
[13] S. Liu, L. Xie, J. Liu, G. Liu, H. Zhong, Y. Wang, H. Zeng, Probing the interactions of hydroxamic acid and mineral surfaces: Molecular mechanism underlying the selective separation, Chem. Eng. J. 374 (2019) 123-132.
[14] P. Wang, W. Qin, L. Ren, Q. Wei, R. Liu, C. Yang, S. Zhong, Solution chemistry and utilization of alkyl hydroxamic acid in flotation of fine cassiterite, Trans. Nonferrous Met. Soc. China. 23 (2013) 1789-1796.
[15] X. Luo, S. Zhu, J. Wang, C. Wang, M. Wu, Characterization and computation of Yb/TiO_2 and its photocatalytic degradation with benzohydroxamic acid, Int J Environ Res Public Health. 114 (2017) 1471.

[16] X. Huang and X. Wang, Toxicity change patterns and its mechanism during the degradation of nitrogen-heterocyclic compounds by O_3/UV, Chemosphere. 69 (2007) 747-754.
[17] E. Lipczynska-Kochany, The photolability of hydroxamic acids and its importance to the human environment, Sci. Total Environ. 100 (1991) 469-482.
[18] C. Wang, T. Zeng, S. Zhu, C. Gu, Synergistic mechanism of rare-earth modification TiO_2 and photodegradation on benzohydroxamic acid, Appl. Sci. 9 (2019) 339.
[19] H. Cheng, H. Lin, H. Huo, Y. Dong, Q. Xue, L. Cao, Continuous removal of ore floatation reagents by an anaerobic–aerobic biological filter, Bioresour. Technol. 114 (2012) 255-261.
[20] H. Wei, B. Gao, J. Ren, A. Li, H. Yang, Coagulation/flocculation in dewatering of sludge: A review, Water Res. 143 (2018) 608-631.
[21] C. Lu, J. Yao, T. Š. Knudsen, M. Amdea, J. Gu, J. Liu, H. Li, J. Zhang, Degradation of α-nitroso-β-naphthol by UVA-B activated peroxide, persulfate and monopersulfate oxidants in water, J. Clean. Prod. 238 (2019) 117942.
[22] A. V.Karim, A. Hassani, P. Eghbali, P. V. Nidheesh, Nanostructured modified layered double hydroxides (LDHs)-based catalysts: A review on synthesis, characterization, and applications in water remediation by advanced oxidation processes, Curr. Opin. Solid State Mat. Sci. 26 (2022) 100965.
[23] F. Ghanbari, Q. Wang, A. Hassani, S. Wacławek, J. Rodríguez-Chueca, K. A. Lin, Electrochemical activation of peroxides for treatment of contaminated water with landfill leachate: Efficacy, toxicity and biodegradability evaluation, Chemosphere. 279 (2021) 130610.
[24] Y. Zhang, J. Zhang, Y. Xiao, V. W. C. Chang, T. Lim, Kinetic and mechanistic investigation of azathioprine degradation in water by UV, UV/H2O2 and UV/persulfate, Chem. Eng. J. 302 (2016) 526-534.
[25] R. Zhang, P. Sun, T. H. Boyer, L. Zhao, C. Huang, Degradation of pharmaceuticals and metabolite in synthetic human urine by UV, UV/H_2O_2, and UV/PDS, Environ. Sci. Technol. 49 (2015) 3056-3066.
[26] X. Zhou, D. Liu, Y. Zhang, J. Chen, H. Chu, Y. Qian, Degradation mechanism and kinetic modeling for UV/peroxydisulfate treatment of penicillin antibiotics, Chem. Eng. J. 341 (2018) 93-101.
[27] S. Madihi-Bidgoli, S. Asadnezhad, A. Yaghoot-Nezhad, A. Hassani, Azurobine degradation using Fe2O3@multi-walled carbon nanotube activated peroxymonosulfate (PMS) under UVA-LED irradiation: performance, mechanism and environmental application, J. Environ. Chem. Eng. 9 (2021) 106660.
[28] A. Hassani, P. Eghbali, B. Kakavandi, K. A. Lin, F. Ghanbari, Acetaminophen removal from aqueous solutions through peroxymonosulfate activation by CoFe2O4/mpg-C3N4 nanocomposite: Insight into the performance and degradation kinetics, Environ. Technol. Innov. 20 (2020) 101127.
[29] L. Fan, F. Tian, B. Xu, W. Ye, Y. Gao, C. Chen, H. Xing, B. Wang, M. Xie, X. Hu, A comparative study on the degradation of phenylurea herbicides by UV/persulfate process: Kinetics, mechanisms, energy demand and toxicity evaluation associated with DBPs, Chem. Eng. J. 428 (2022) 132088.
[30] W. Huang, A. Bianco, M. Brigante, G. Mailhot, UVA-UVB activation of hydrogen peroxide and persulfate for advanced oxidation processes: Efficiency, mechanism and effect of various water constituents, J. Hazard. Mater. 347 (2018) 279-287.

[31] A. Gabet, H. Métivier, C. Brauer, G. Mailhot, M. Brigante, Hydrogen peroxide and persulfate activation using UVA-UVB radiation: Degradation of estrogenic compounds and application in sewage treatment plant waters, J. Hazard. Mater. 405 (2021) 124693.
[32] F. Neese, The ORCA program system, WIREs Comput. Mol. Sci. 2 (2012) 73-78.
[33] F. Neese, Software update: the ORCA program system, version 4.0, Wires Comput. Mol. Sci. 8 (2017) 73-78.
[34] T. Lu and F. Chen, Multiwfn: A multifunctional wavefunction analyzer, J. Comput. Chem. 33 (2012) 580-592.
[35] Z. Chen, J. Yao, T. Š. Knudsen, B. Ma, B. Liu, H. Li, X. Zhu, C. Zhao, W. Pang, Y. Cao, Degradation of novel mineral flotation reagent 8-hydroxyquinoline by superparamagnetic immobilized laccase: Effect, mechanism and toxicity evaluation, Chem. Eng. J. 382 (2020) 122312.
[36] ECOSAR, www.epa.gov/oppt/newchems/tools/21ecosar.htm, (2014).
[37] D. Prabhakaran, P. Sukul, M. Lamshoft, M. A. Maheswari, S. Zühlke, M. Spiteller, Photolysis of difloxacin and sarafloxacin in aqueous systems, Chemosphere. 77 (2009) 739-746.
[38] Y. Ji, Y. Yang, L. Zhou, L. Wang, J. Lu, C. Ferronato, J. Chovelon, Photodegradation of sulfasalazine and its human metabolites in water by UV and UV/peroxydisulfate processes, Water Res. 133 (2018) 299-309.
[39] Y. Zhang, Y. Xiao, Y. Zhong, T. Lim, Comparison of amoxicillin photodegradation in the UV/H_2O_2 and UV/persulfate systems: Reaction kinetics, degradation pathways, and antibacterial activity, Chem. Eng. J. 372 (2019) 420-428.
[40] D. E. Latch, J. L. Packer, W. A. Arnold, K. McNeill, Photochemical Conversion of Triclosan to 2,8-Dichlorodibenzo-p-dioxin in Aqueous Solution, J. Photochem. Photobiol. A-Chem. 158 (2003) 63-66.
[41] R. Chapleski Jr, A. Chowdhury, A. Wanhala, V. Bocharova, S. Roy, P. Keller, D. Everly, S. Jansone-Popova, A. Kisliuk, R. Sacci, A. Stack, C. Anderson, B. Doughty, V. Bryantsev, A Molecular-Scale Approach to Rare-Earth Beneficiation: Thinking Small to Avoid Large Losses, iScience. 23 (2020) 101435.
[42] C. Tan, N. Gao, Y. Deng, Y. Zhang, M. Sui, J. Deng, S. Zhou, Degradation of antipyrine by UV, UV/H_2O_2 and UV/PS, J. Hazard. Mater. 260 (2013) 1008-1016.
[43] D. Wen, W. Li, J. Lv, Z. Qiang, M. Li, Methylene blue degradation by the VUV/UV/persulfate process: Effect of pH on the roles of photolysis and oxidation, J. Hazard. Mater. 391 (2020) 121855.
[44] N. T. Hoang, V. T. Nguyen, N. D. M. Tuan, T. D. Manh, P. Le, D. V. Tac, F. M. Mwazighe, Degradation of dyes by UV/Persulfate and comparison with other UV-based advanced oxidation processes: Kinetics and role of radicals, Chemosphere. 8 (2022) 134197.
[45] Z. Yang, H. Chen, J. Wang, R.Yuan, F. Wang, B. Zhou, Efficient degradation of diisobutyl phthalate in aqueous solution through electro-Fenton process with sacrificial anode, J. Environ. Chem. Eng. 8 (2020) 104057.
[46] Y. Liu, X. He, Y. Fu, D. D. Dionysiou, Degradation kinetics and mechanism of oxytetracycline by hydroxyl radical-based advanced oxidation processes, Chem. Eng. J. 284 (2016) 1317-1327.
[47] T. Chen, J. Ma, Q. Zhang, Z. Xie, Y. Zeng, R. Li, H. Liu, Y. Liu, W. Lv, G. Liu, Degradation of propranolol by UV-activated persulfate oxidation: Reaction kinetics, mechanisms, reactive sites, transformation pathways and Gaussian calculation, Sci. Total Environ. 690 (2019) 878-890.

[48] Y. Zhou, C. Chen, K. Guo, Z. Wu, L. Wang, Z. Hua, J. Fang, Kinetics and pathways of the degradation of PPCPs by carbonate radicals in advanced oxidation processes, Water Res. 185 (2020) 116231.
[49] J. Wang, S. Wang, Effect of inorganic anions on the performance of advanced oxidation processes for degradation of organic contaminants, Chem. Eng. J. 411 (2021) 128392.
[50] J. Peuravuori and K. Pihlaja, Phototransformations of selected pharmaceuticals under low-energy UVA–vis and powerful UVB–UVA irradiations in aqueous solutions—the role of natural dissolved organic chromophoric material, Anal Bioanal Chem. 394 (2009) 1621-1636.
[51] Y. Peng, H. Shi, Z. Wang, Y. Fu, Y. Liu, Kinetics and reaction mechanism of photochemical degradation of diclofenac by UV-activated peroxymonosulfate, RSC Adv. 11 (2021) 6804-6817.
[52] A. Cai, J. Deng, T. Zhu, C. Ye, J. Li, S. Zhou, Q. Li, X. Li, Enhanced oxidation of carbamazepine by UV-LED/persulfate and UV-LED/H_2O_2 processes in the presence of trace copper ions, Chem. Eng. J. 404 (2021) 127119.
[53] M. Lee, W. Wang, Y. Du, H. Hua, N. Huang, Z. Xu, Q. Wu, B. Ye, Enhancement effect among a UV, persulfate, and copper (UV/PS/Cu^{2+}) system on the degradation of nonoxidizing biocide: The kinetics, radical species, and degradation pathway, Chem. Eng. J. 382 (2020) 122312.
[54] G. P. Anipsitakis and D. D. Dionysiou, Radical Generation by the Interaction of Transition Metals with Common Oxidants, Environ. Sci. Technol. 38 (2004) 3705-3712.
[55] L. Lian, B. Yao, S Hou, J Fang, S Yan, W. Song, Kinetic study of hydroxyl and sulfate radical-mediated oxidation of pharmaceuticals in wastewater effluents, Environ. Sci. Technol. 51 (2017) 2954-2962.
[56] M. Dou, J. Wang, B. Gao, C. Xu, F. Yang, Photocatalytic difference of amoxicillin and cefotaxime under visible light by mesoporous g-C3N4: Mechanism, degradation pathway and DFT calculation, Chem. Eng. J. 383 (2020) 123134.
[57] Y. Bao, S. Deng, X. Jiang, Y. Qu, Y. He, L. Liu, Q. Chai, M. Mumtaz, Jun Huang, G. Cagnetta, G. Yu, Degradation of PFOA Substitute: GenX (HFPO–DA Ammonium Salt): Oxidation with UV/Persulfate or Reduction with UV/Sulfite? Environ. Sci. Technol. 52 (2018) 11728-11734.
[58] A. Kaczor, J. Szczepanski, M. Valab, L. M. Proniewicz, Matrix-isolation and computational study of salicylhydroxamic acid and its photochemical degradation, Phys. Chem. Chem. Phys. 7 (2005) 1960-1965.
[59] Y. Liu, X. He, Y. Fu, D. D. Dionysiou, Kinetics and mechanism investigation on the destruction of oxytetracycline by UV-254 nm activation of persulfate, J. Hazard. Mater. 305 (2016) 229-239.
[60] M. Lee, W. Wang, Q. Wu, N. Huang, Z. Xu, H. Hu, Degradation of dodecyl dimethyl benzyl ammonium chloride (DDBAC) as a non-oxidizing biocide in reverse osmosis system using UV/persulfate: Kinetics, degradation pathways, and toxicity evaluation, Chem. Eng. J. 352 (2018) 283-292.
[61] Y. Lee, G. Lee, K. Zoh, Benzophenone-3 degradation via UV/H_2O_2 and UV/persulfate reactions, J. Hazard. Mater. 403 (2021) 123591.
[62] Z. Wang, W. Zhang, H. Wang, Z. Wang, J. Chang, Oxidation of acetylsalicylic acid in water by UV/O_3 process: Removal, byproduct analysis, and investigation of degradation mechanism and pathway, J. Environ. Chem. Eng. 9 (2021) 106259.
[63] S. Ding, J. Wan, Y. Wang, Z. Yan, Y. Ma, Activation of persulfate by molecularly imprinted Fe-MOF-74@SiO2 for the targeted degradation of dimethyl

phthalate: Effects of operating parameters and chlorine, Chem. Eng. J. 422 (2021) 130406.
[64] N.H. Trang, E. Kwon, G. Lisak, C. Hu, K. A. Lin, Cobalt ferrite nanoparticle-loaded nitrogen-doped carbon sponge as a magnetic 3D heterogeneous catalyst for monopersulfate-based oxidation of salicylic acid, Chemosphere. 267 (2021) 128906.
[65] G.Albarran and R.H.Schuler, Concerted effects in the reaction of •OH radicals with aromatics: radiolytic oxidation of salicylic acid, Radiat. Phys. Chem. 67 (2003) 279-285.
[66] J. Lv, S. Zhang, S. Wang, L. Luo, D. Cao, P. Christie, Molecular-Scale Investigation with ESI-FT-ICR-MS on Fractionation of Dissolved Organic Matter Induced by Adsorption on Iron Oxyhydroxides, Environ. Sci. Technol. 50 (2016) 2328-2336.
[67] R. Zhang, Y. Yang, C. Huang, N. Li, H. Liu, L. Zhao, P. Sun, UV/H2O2 and UV/PDS Treatment of Trimethoprim and Sulfamethoxazole in Synthetic Human Urine: Transformation Products and Toxicity, Environ. Sci. Technol. 50 (2016) 2573-2583.
[68] M. Xu, J. Deng, A. Cai, C. Ye, X. Ma, Q. Li, S. Zhou, X. Li, Synergistic effects of UVC and oxidants (PS vs. Chlorine) on carbamazepine attenuation: Mechanism, pathways, DBPs yield and toxicity assessment, Chem. Eng. J. 413 (2021) 127533.

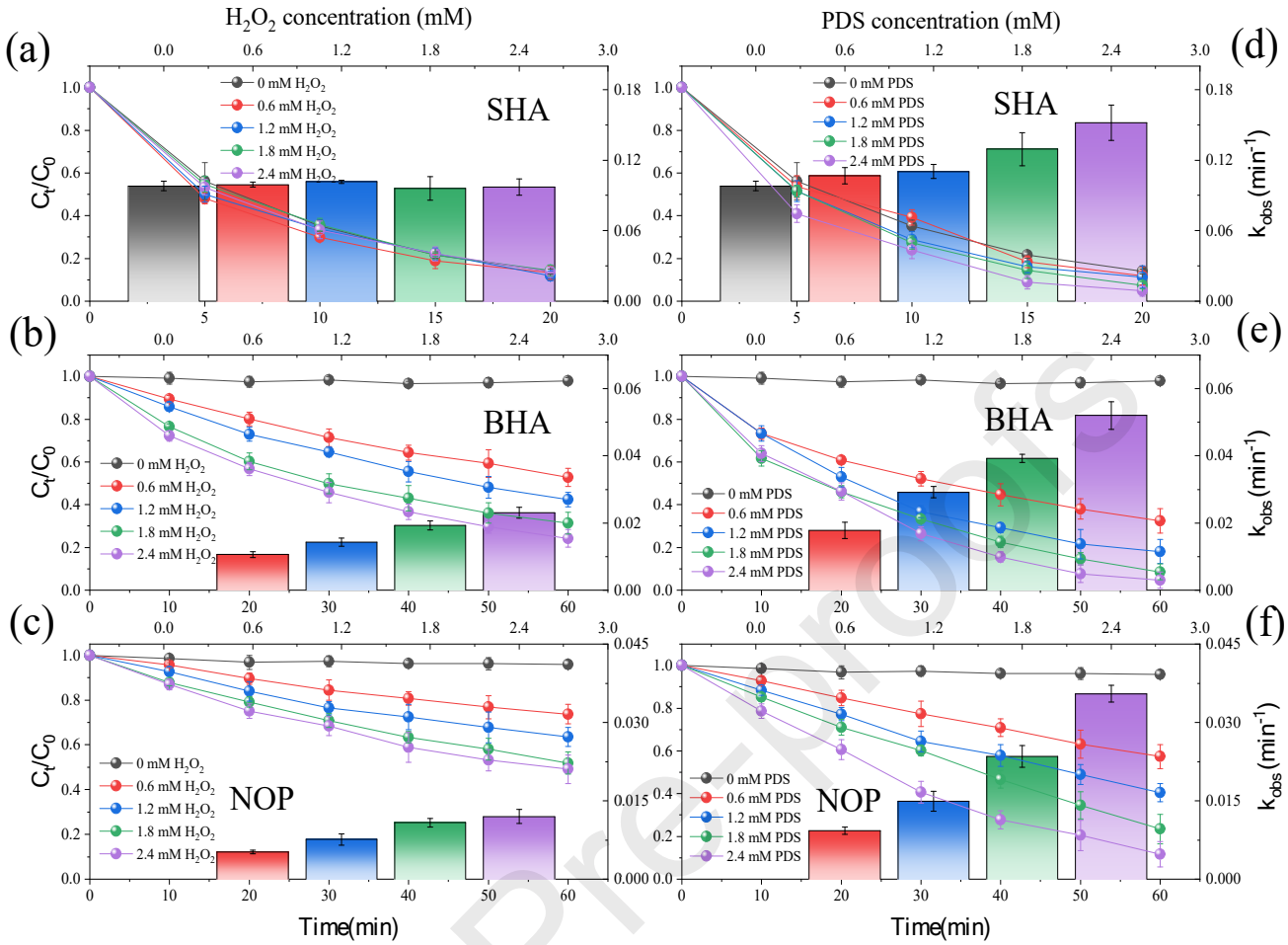

Fig. 1. The degradation kinetics and rate constant of SHA (a), BHA (b) and NOP (c) in the UVA-B/H_2O_2 system; The degradation kinetics and rate constant of SHA (d), BHA (e) and NOP (f) in the UVA-B/PDS system; Experimental conditions: $[SHA]_0 = [BHA]_0 = [NOP]_0 = 60$ μM, $[Oxidant]_0 = 0$ - 2.4 mM, pH = 7.0.

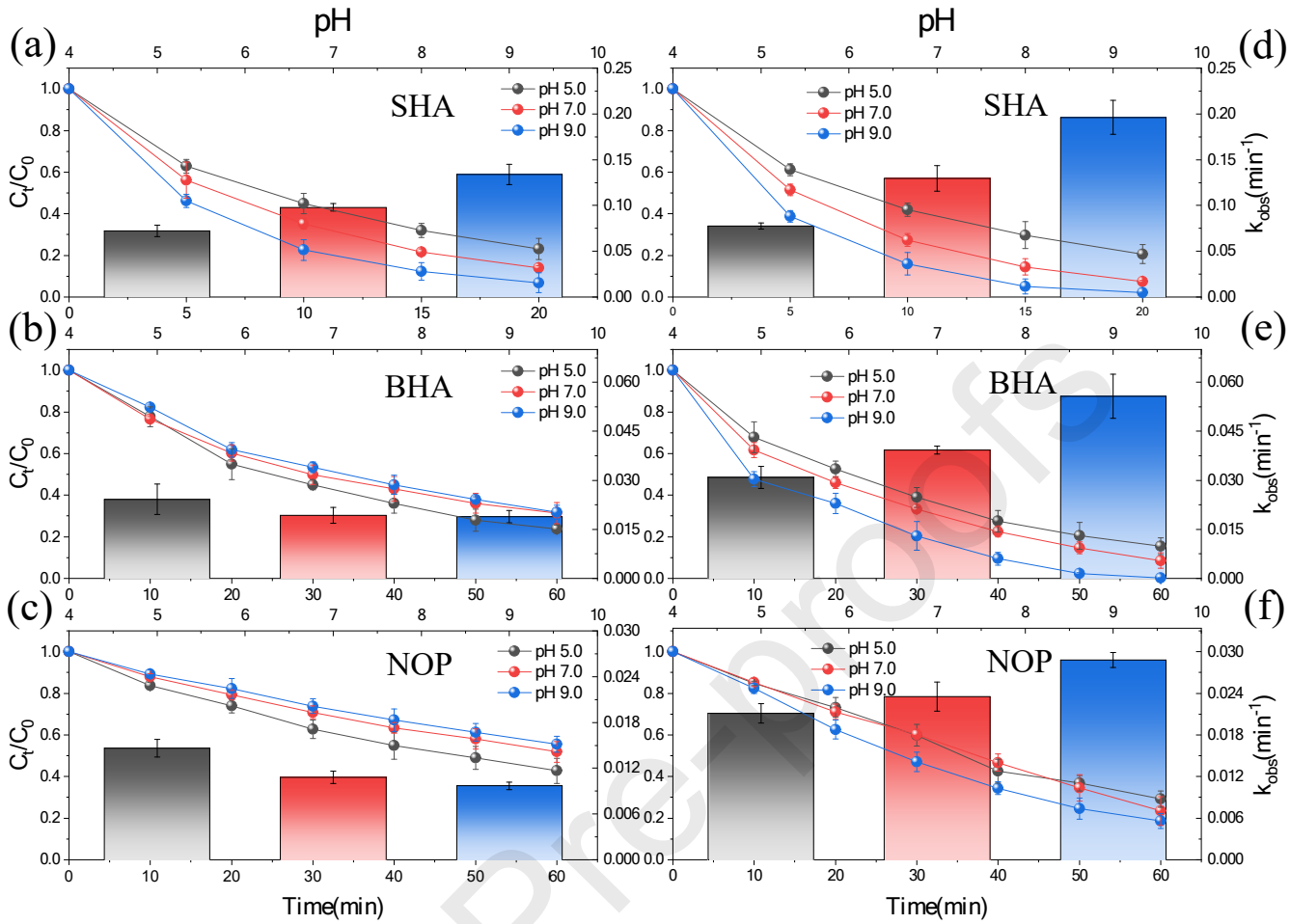

Fig. 2. Effect of pH on the degradation of SHA (a) in the UVA-B only system; Degradation of BHA (b) and NOP (c) in the UVA-B/H_2O_2 system; Degradation of SHA (d), BHA (e) and NOP (f) in the UVA-B/PDS system; Experimental conditions: $[SHA]_0 = [BHA]_0 = [NOP]_0 = 60$ μM, $[Oxidant]_0 = 1.8$ mM, pH = 5.0 - 9.0.

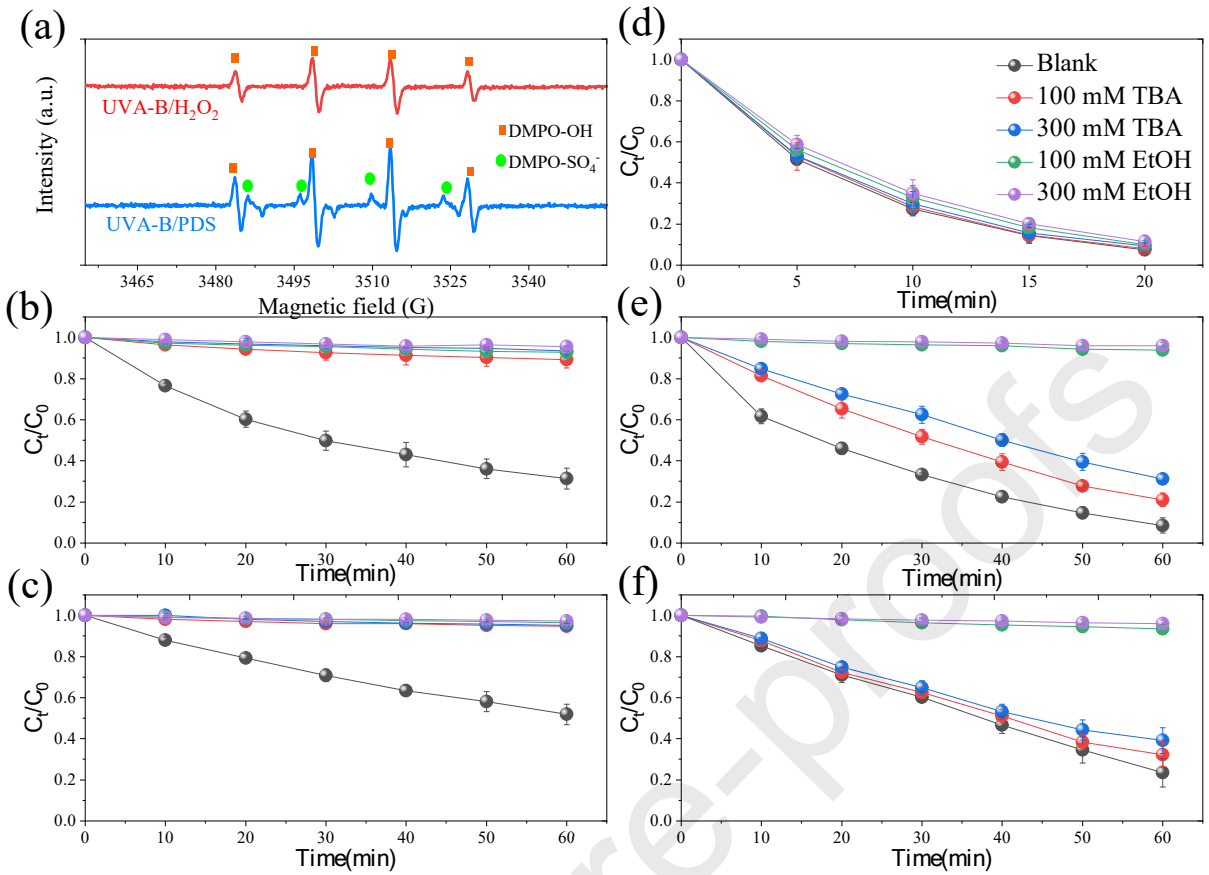

Fig. 3. ESR spectrum of UVA-B/AOP systems under DMPO capture agent (a); Effect of free radical scavenger in the degradation of BHA (b) and NOP (c) in the UVA-B/H_2O_2 system; Effect of free radical scavenger in the degradation of SHA (d), BHA (e) and NOP (f) in the UVA-B/PDS system. Experimental conditions: $[SHA]_0$ = $[BHA]_0$ = $[NOP]_0$ = 60 μM, $[Oxidant]_0$ = 1.8 mM, pH = 7.0.

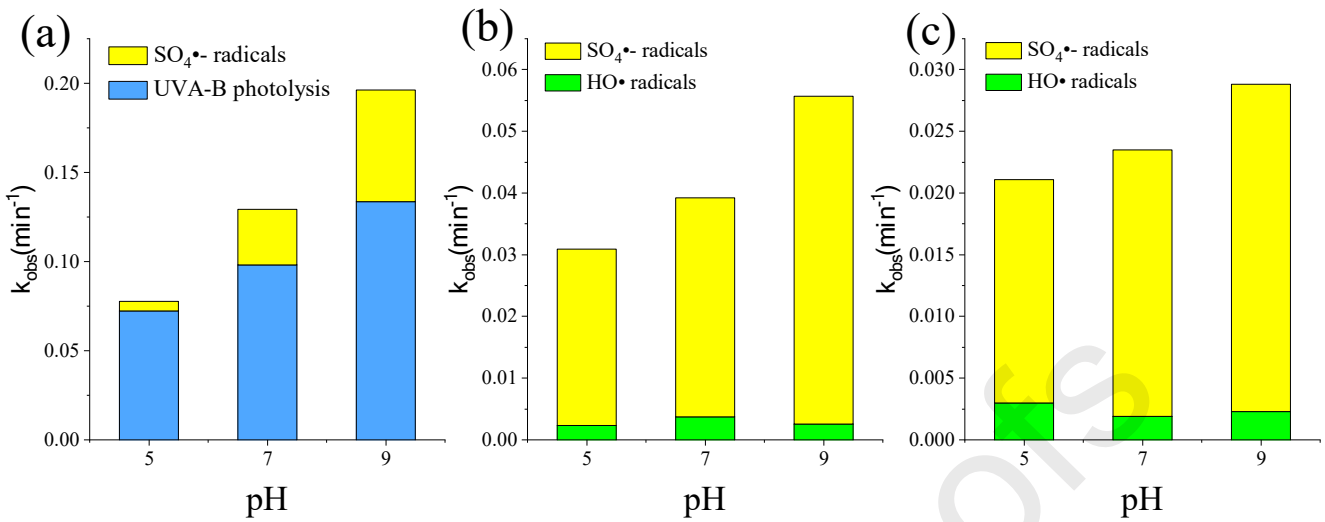

Fig. 4. Relative contributions of radicals to the degradation of SHA (a), BHA (b) and NOP (c) in the UVA-B/PDS reactions. Experimental conditions: $[SHA]_0 = [BHA]_0 = [NOP]_0 = [NB]_0 = [BA]_0 = 60$ μM, $[Oxidant]_0 = 1.8$ mM.

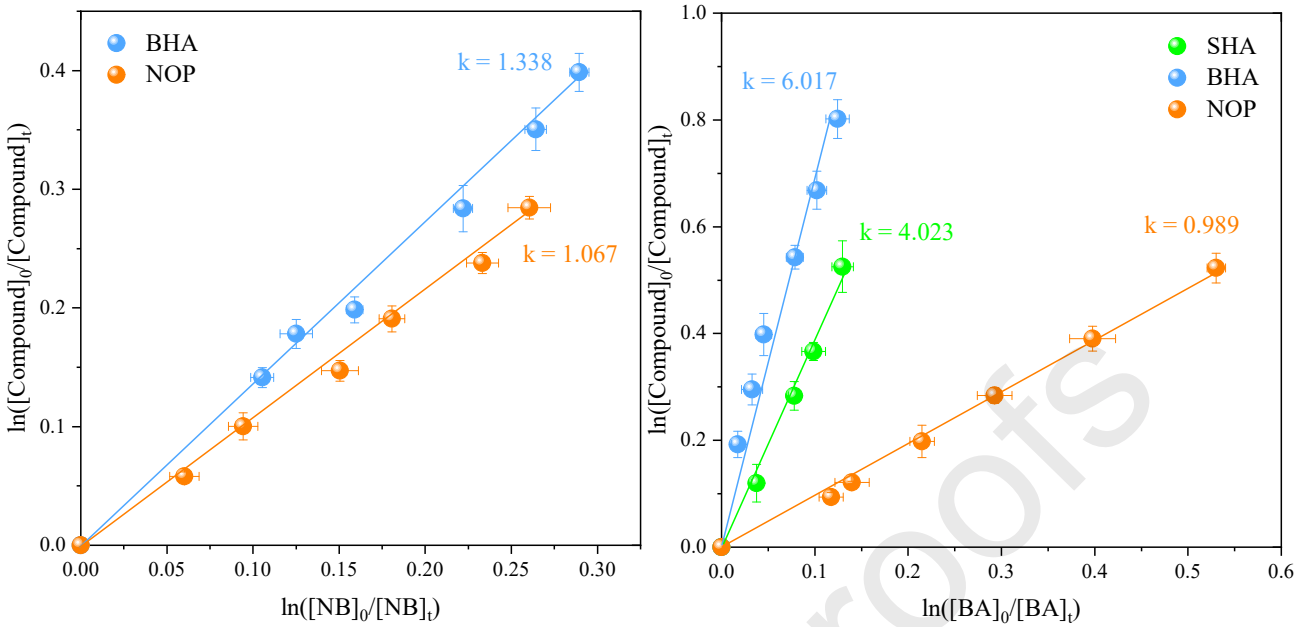

Fig. 5. Determination of the second-order rate constants of the reactions of $HO^{\bullet}$ (a) and $SO_4^{\bullet-}$ (b) with HAAs; Experimental conditions: $[SHA]_0 = [BHA]_0 = [NOP]_0 = [NB]_0 = [BA]_0 = 60$ μM, $[Oxidant]_0 = 1.8$ mM, pH = 7.0.

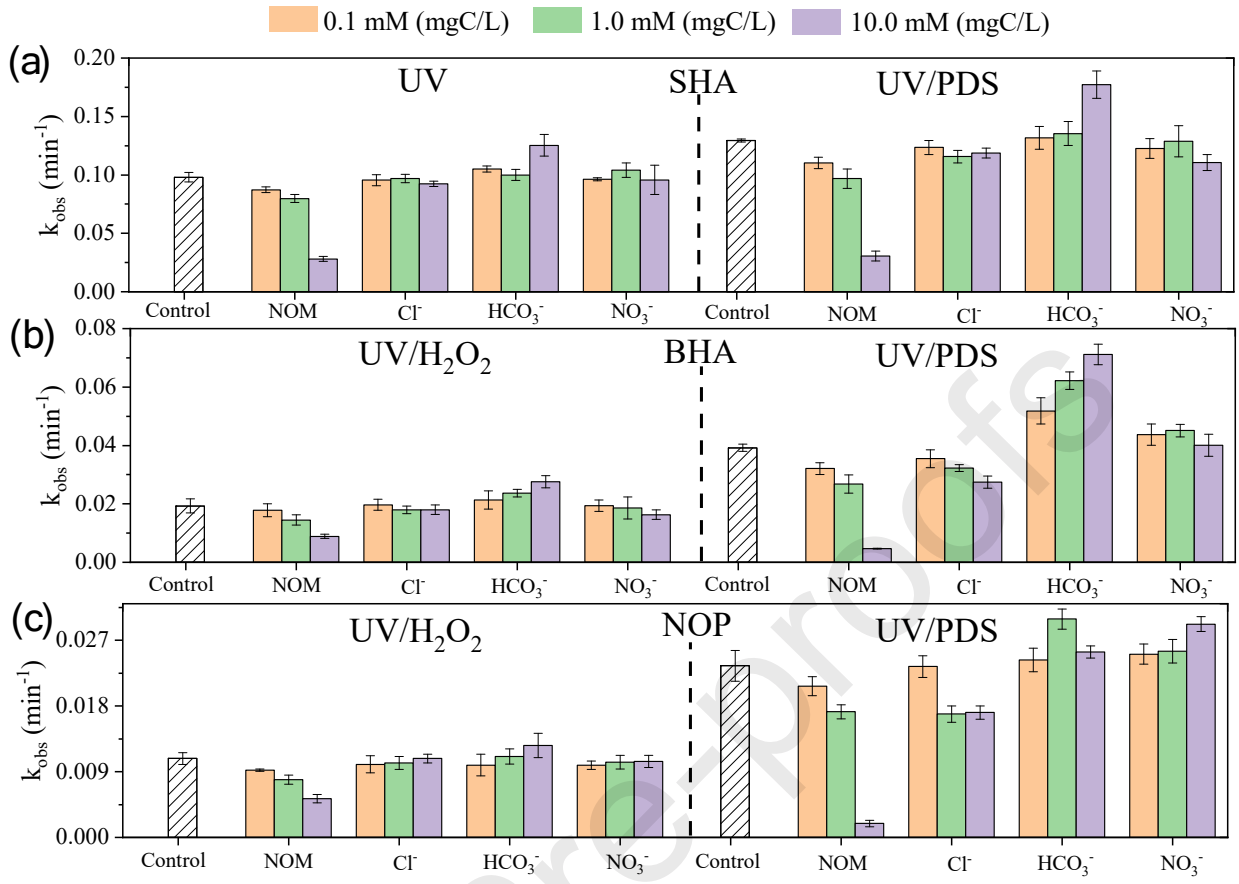

Fig. 6. Influence of NOM and inorganic anion on degradation of SHA (a), BHA (b) and NOP (c) in the UVA-B/AOP system. Experimental conditions: $[SHA]_0 = [BHA]_0 = [NOP]_0 = 60$ μM, $[Oxidant]_0 = 1.8$ mM, and pH 7.0.

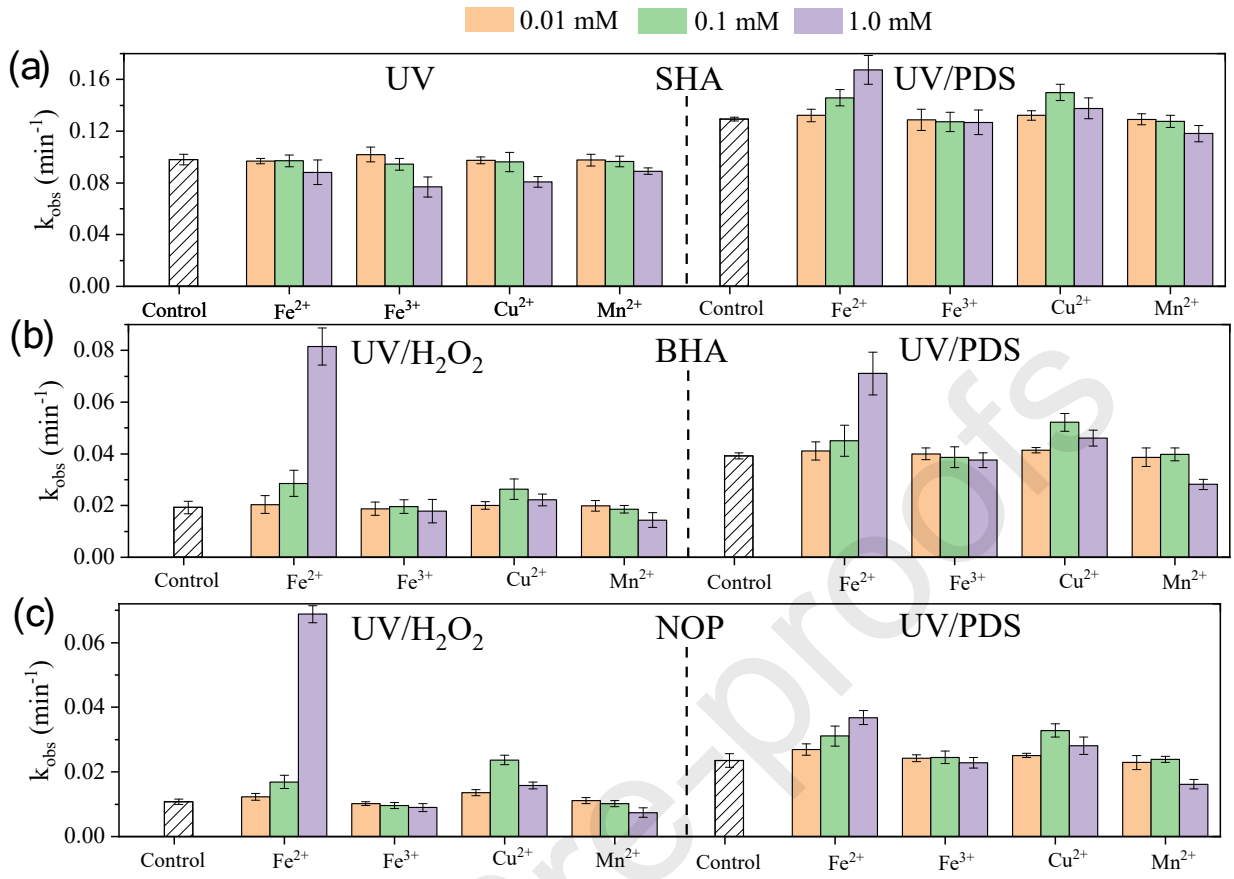

Fig. 7. Effect of inorganic cations on degradation of SHA (a), BHA (b) and NOP (c); Experimental conditions: $[SHA]_0 = [BHA]_0 = [NOP]_0 = 60$ μM, $[Oxidant]_0 = 1.8$ mM, and pH 7.0.

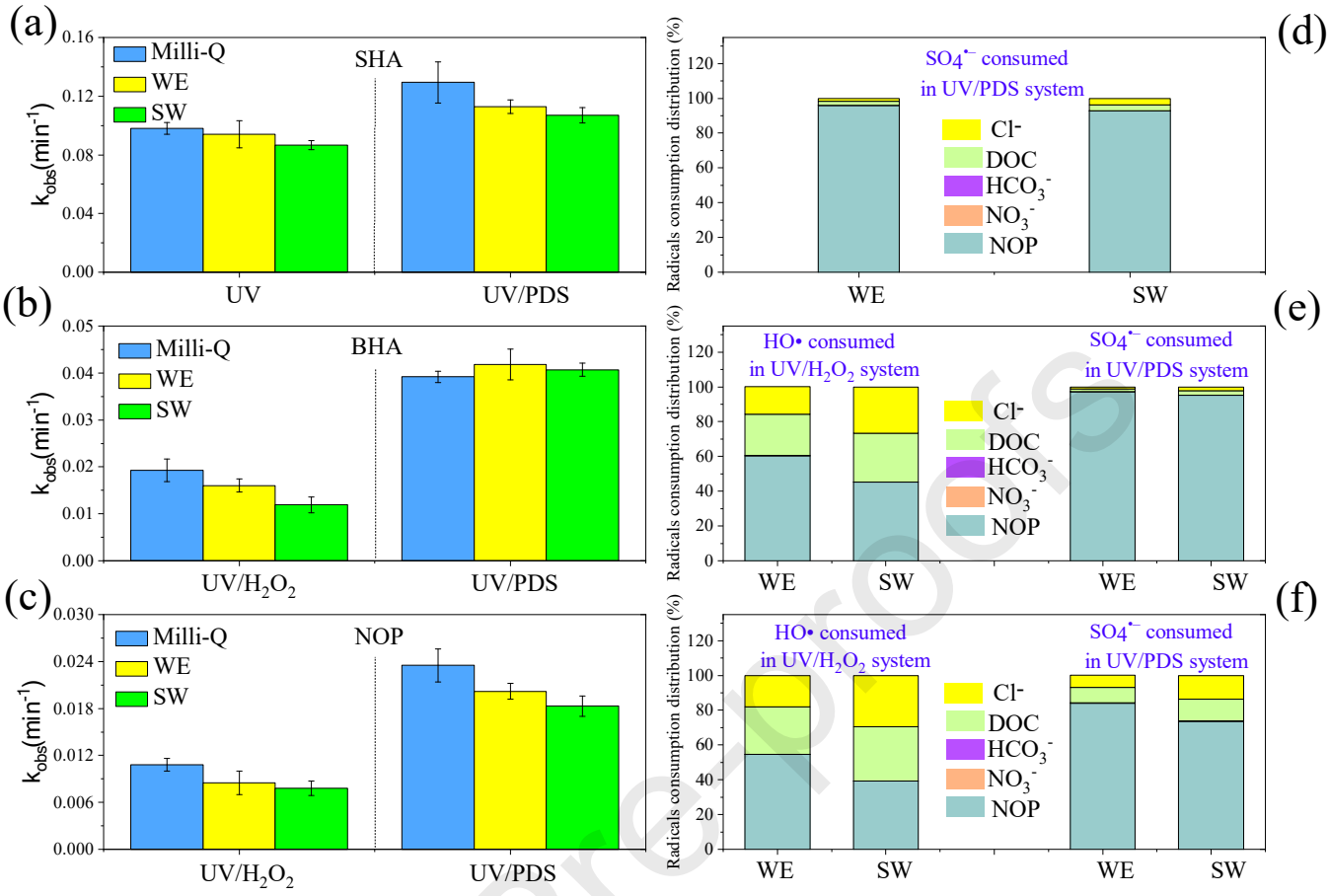

Fig. 8. SHA (a), BHA (b) and NOP (c) degradation rate constants in Milli-Q water and two real waters by the UVA-B/AOP; Fractions of $HO^{\bullet}$ and $SO_4^{\bullet-}$ consumed by major matrix components during SHA (d), BHA (e) and NOP (f) degradation in two waters using the UVA-B/AOP; Experimental conditions: $[SHA]_0$ = $[BHA]_0$ = $[NOP]_0$ = 60 μM, $[Oxidant]_0$ = 1.8 mM.

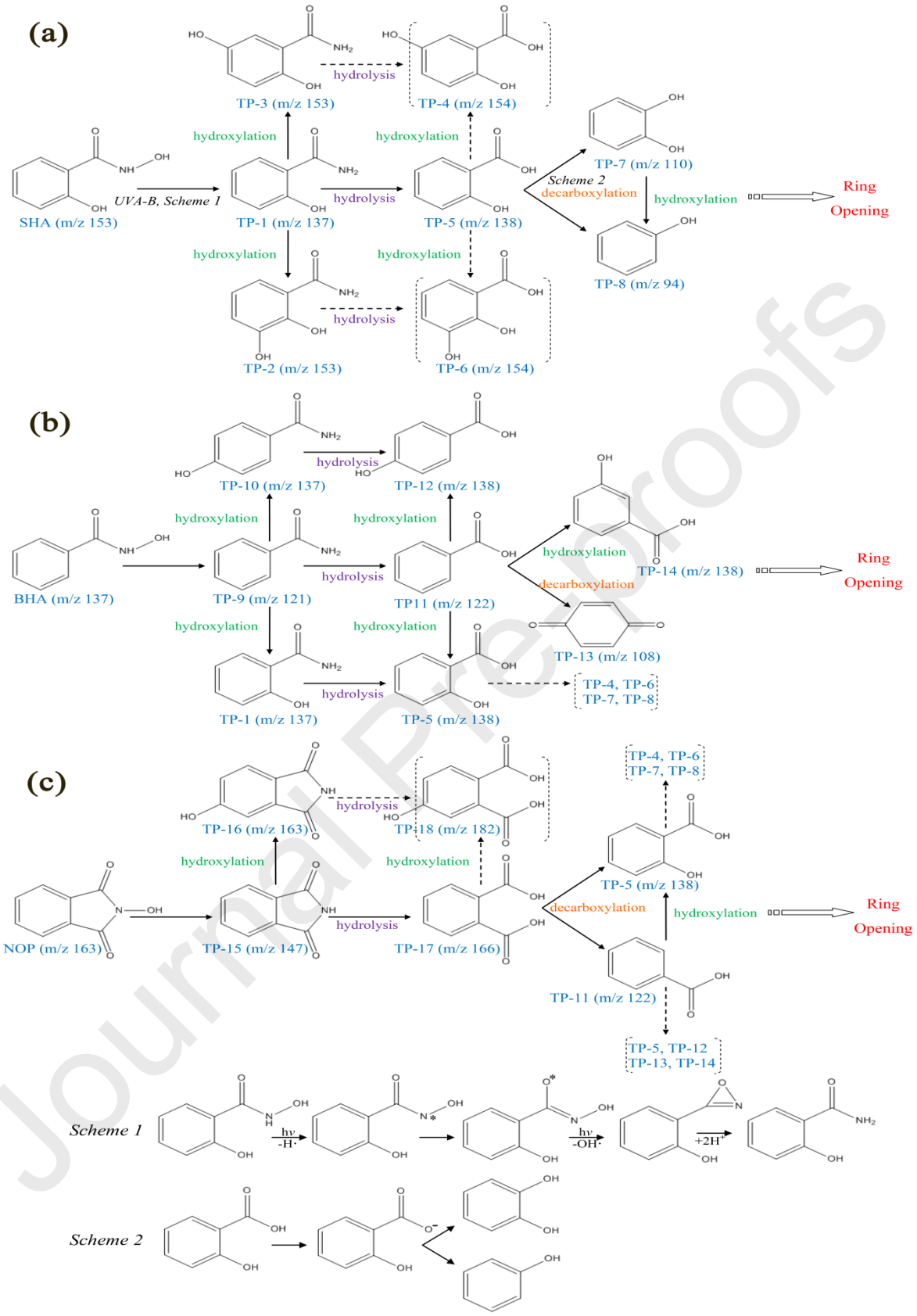

Fig. 9. The proposed pathway for SHA (a), BHA (b) and NOP (c) degradation in the UVA-B/AOP system.

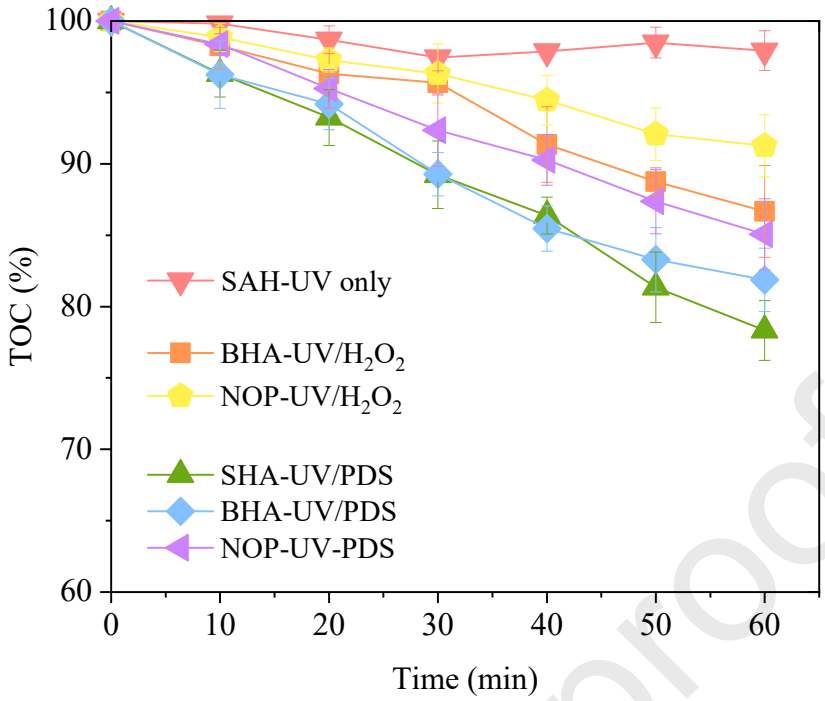

Fig. 10. Mineralization of HAA in the UVA-B/AOP systems.

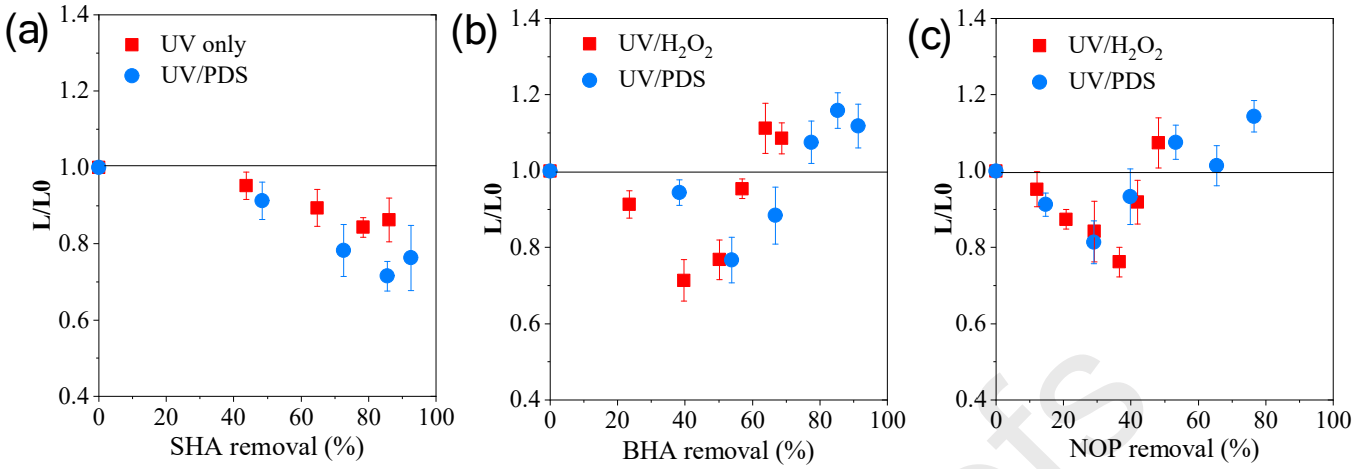

Fig. 11. Influence on Vibrio fischeri bioluminescence by SHA (a), BHA (b) and NOP (c) after different treatments. Experimental conditions: $[SHA]_0$ = $[BHA]_0$ = $[NOP]_0$ = 60 μM, $[Oxidant]_0$ = 1.8 mM, and pH 7.0.

Table 1 Economic comparison of UV/AOP for HAA degradation ($[HAA]_0$ = 60 μM, $[H_2O_2]$ = [PDS] = 1.8 mM, and pH 7.0).

	Oxidation processes	EE/O_{UV} (kWh L^{-1}) x 10^{-2} [a]	$EE/O_{oxidant}$ (kWh L^{-1}) x 10^{-2} [b]	EE/O^{total} (kWh L^{-1}) x 10^{-2}
SHA	UV	2.34	0.11	2.45
BHA	UV/H_2O_2	11.92	0.18	12.10
NOP	UV/H_2O_2	21.04	0.32	21.36
SHA	UV/PDS	1.77	0.29	2.06
BHA	UV/PDS	5.62	0.30	5.92
NOP	UV/PDS	9.53	0.51	10.04

[a]\$0.10 kWh^{-1} (U.S. Energy Information Administration, 2015).
[b]PS: \$0.74 kg^{-1} (\$0.18 mol^{-1}); H_2O_2: \$1.5 kg^{-1} (\$0.051 mol^{-1}).

Highlights

- Direct photolysis' contribution to SHA removal was much higher than that of $HO^{\bullet}$ and $SO_4^{\bullet-}$.
- Second-order rate constant of three HAAs with $HO^{\bullet}$ and $SO_4^{\bullet-}$ were determined.
- At pH 5.0-9.0, the degradation of BHA and NOP were always dominated driven by $SO_4^{\bullet-}$.
- DFT calculation was applied to predict the reactive sites and degradation pathways.
- Hydrolysis, hydroxylation, decarboxylation and ring opening were the main pathways.